JCB Journal of Cell Biology

ARTICLE

Microtubules promote intercellular contractile force transmission during tissue folding

Clint S. Ko, Vardges Tserunyan, and Adam C. Martin

During development, forces transmitted between cells are critical for sculpting epithelial tissues. Actomyosin contractility in the middle of the cell apex (medioapical) can change cell shape (e.g., apical constriction) but can also result in force transmission between cells via attachments to adherens junctions. How actomyosin networks maintain attachments to adherens junctions under tension is poorly understood. Here, we discovered that microtubules promote actomyosin intercellular attachments in epithelia during *Drosophila melanogaster* mesoderm invagination. First, we used live imaging to show a novel arrangement of the microtubule cytoskeleton during apical constriction: medioapical Patronin (CAMSAP) foci formed by actomyosin contraction organized an apical noncentrosomal microtubule network. Microtubules were required for mesoderm invagination but were not necessary for initiating apical contractility or adherens junction assembly. Instead, microtubules promoted connections between medioapical actomyosin and adherens junctions. These results delineate a role for coordination between actin and microtubule cytoskeletal systems in intercellular force transmission during tissue morphogenesis.

Introduction

Apical constriction is a ubiquitous cell-shape change that results in dramatic rearrangements of tissue architecture, such as tissue folding (Sawyer et al., 2010; Heisenberg and Bellaïche, 2013; Martin and Goldstein, 2014). The cellular force necessary to constrict a cell apex is generated by actomyosin contraction, which is regulated by RhoA signaling (Jaffe and Hall, 2005; Kasza and Zallen, 2011; Lecuit et al., 2011). During apical constriction, the apical cortex is often polarized; myosin-II (myosin) is activated near the middle of the apical cortex (medioapical), which contracts an actin filament (F-actin) network that spans the apical surface (Sawyer et al., 2009; Blanchard et al., 2010; David et al., 2010; Mason et al., 2013; Booth et al., 2014; Sánchez-Corrales et al., 2018). In order for these changes in cell geometry to cause tissue morphogenesis, cellular forces must be transmitted and integrated across the tissue (Fernandez-Gonzalez et al., 2009; Lecuit and Yap, 2015). This is mediated by connecting contractile actomyosin meshworks to E-cadherin–based adherens junctions (Martin et al., 2010; Sawyer et al., 2011). Molecular components that mediate this linkage have been identified and are important for morphogenesis (Sawyer et al., 2009; Desai et al., 2013). In addition, this attachment has been shown to be dynamic and actin turnover is required to promote attachment by repairing lost connections (Roh-Johnson et al., 2012; Jodoin et al., 2015). However, whether other mechanisms maintain actomyosin network connections to junctions, in the face of tension, remains unknown.

During gastrulation in the early *Drosophila melanogaster* embryo, apical constriction leads to mesoderm and endoderm cell invagination (Leptin and Grunewald, 1990; Sweeton et al., 1991; Fig. 1 A). Mesoderm cells express transcription factors (Twist and Snail) that promote apical RhoA activation, which induces actomyosin contractility (Barrett et al., 1997; Häcker and Perrimon, 1998; Dawes-Hoang et al., 2005; Fox and Peifer, 2007; Kölsch et al., 2007; Izquierdo et al., 2018). Contractile force is transmitted across the folding tissue through adherens junctions, resulting in epithelial tension predominantly along the anterior–posterior axis (Martin et al., 2010; Chanet et al., 2017). Apical constriction in multiple invagination processes depends on polarized RhoA signaling, with active RhoA and its downstream effector Rho-associated coiled-coil kinase (ROCK), which activates myosin (Amano et al., 1996; Mizuno et al., 1999), being enriched in the middle of the apical surface (Mason et al., 2013; Booth et al., 2014; Coravos and Martin, 2016; Chung et al., 2017). It is poorly understood how intercellular actomyosin connections are promoted when the medioapical pool of active RhoA is present at a distance from cell junctions.

Department of Biology, Massachusetts Institute of Technology, Cambridge, MA.

Correspondence to Adam C. Martin: acmartin@mit.edu.

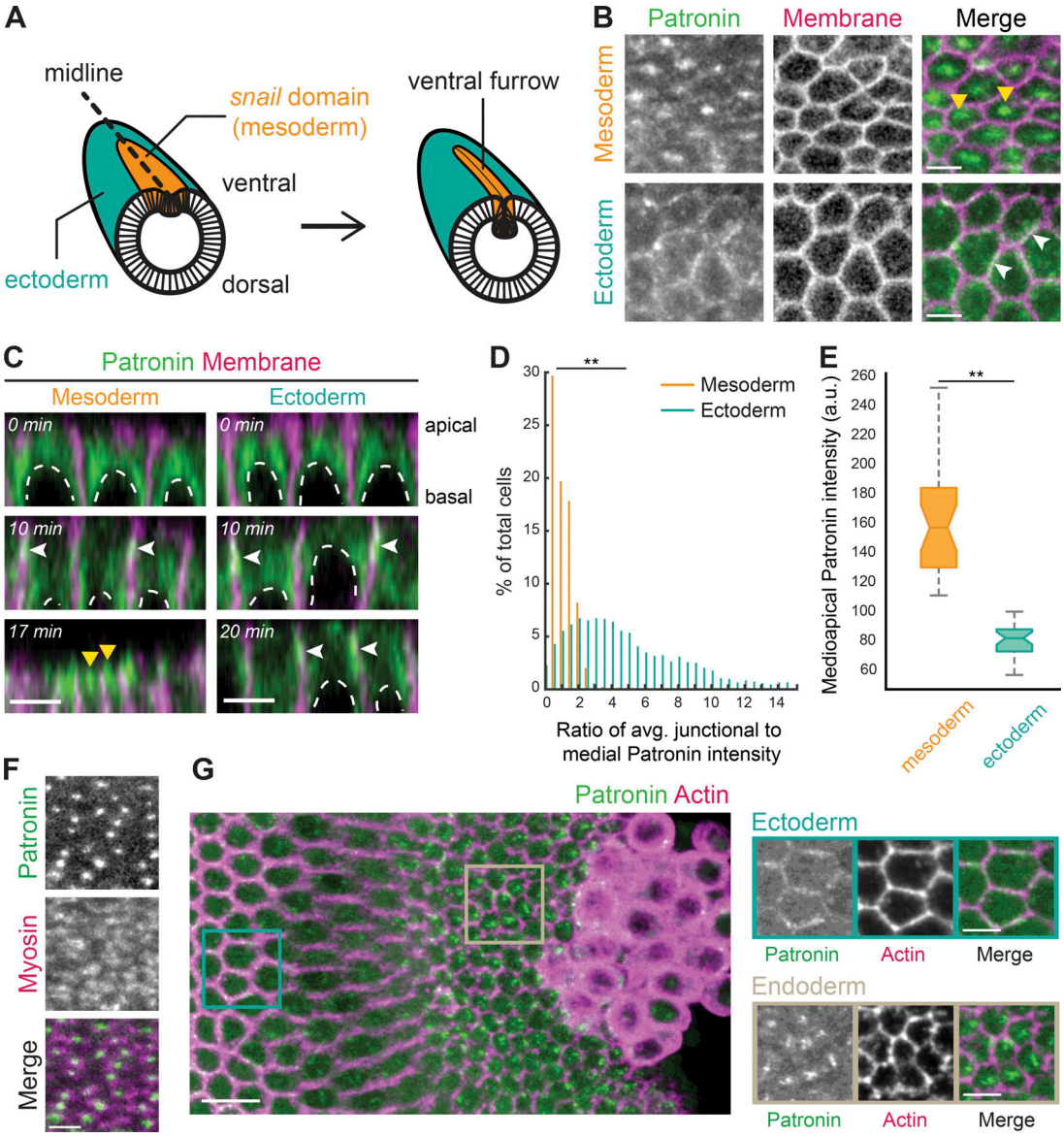

Figure 1. **Patronin::GFP localizes medioapically in apically constricting cells. (A)** Diagram of an embryo undergoing mesoderm invagination. Ventral, mesoderm cells (*snail* expressing domain highlighted in orange) apically constrict and internalize, forming a ventral furrow along the midline (dashed line). **(B)** Patronin::GFP is present in a medioapical focus specifically in the mesoderm (top row, yellow arrowhead). Patronin::GFP is enriched at junctions in the ectoderm (bottom row, white arrowhead). Images are maximum-intensity projections from a live embryo expressing Patronin::GFP (apical surface) and Gap43::mCH (mCherry-tagged plasma membranes, subapical slice). **(C)** Patronin::GFP localization changes from junctional (white arrowheads) to medioapical (yellow arrowheads) in the mesoderm. Images are apical–basal cross sections from a live embryo expressing Patronin::GFP and Gap43::mCH. Top row: mid-cellularization; middle row: late cellularization/early gastrulation; bottom row: during folding. Nuclei are highlighted by dashed white lines. **(D)** Quantification of medioapical Patronin::GFP enrichment. Individual cells were segmented, the junctional and medioapical Patronin::GFP intensity was calculated, and the distribution of the ratio (junctional/medioapical) was plotted as a percentage of cells within each bin (n = 6 embryos, 559 cells; **, $P < 0.0001$, Kolmogorov–Smirnov test). **(E)** Apical Patronin::GFP foci are more intense in the mesoderm than in the ectoderm. The maximum apical Patronin::GFP intensity was determined in a region encompassing the medioapical cortex in both the mesoderm (left) and ectoderm (right; n = 6 embryos, 10 measurements per embryo; **, $P < 0.0001$, unpaired t test). The notch is the median, bottom and top edges of the box are the 25th and 75th percentiles; whiskers extend to the most extreme data points. **(F)** Medioapical Patronin::GFP colocalizes with apical myosin patches. Images are apical surface Z-projections from a representative live embryo expressing Patronin::GFP and Myo::mCH (sqh::mCH). **(G)** Patronin::GFP localizes medioapically in apically constricting endoderm cells. Images are maximum-intensity projections of a fixed embryo expressing Patronin::GFP (apical surface). The embryo was immunostained with Phalloidin conjugated with AF647 to visualize cell outlines (subapical section). Scale bars represent 10 µm (G, left) and 5 µm (B–F and G, right).

While the regulation and organization of actomyosin during apical constriction has been well studied, the organization of the microtubule cytoskeleton and its importance are less well understood. In epithelia, there is evidence for different microtubule functions, such as regulating assembly or position of the adherens junctions (Harris and Peifer, 2005; Stehbens et al., 2006; Meng et al., 2008; Le Droguen et al., 2015), recruiting apical myosin (Booth et al., 2014), regulating RhoA

(Rogers et al., 2004; Nagae et al., 2013), and providing a counterforce resisting actomyosin contraction (Singh et al., 2018; Takeda et al., 2018). Importantly, studies have shown that microtubules are necessary for cell shape changes, like apical constriction (Lee et al., 2007; Lee and Harland, 2007; Booth et al., 2014). However, it is unknown whether microtubules also play additional roles in promoting tissue shape changes, which requires imaging microtubules with high spatial and temporal resolution at both cell and tissue scales.

Here, we investigated microtubule cytoskeleton organization and its mechanistic contribution to mesoderm invagination. We showed that a microtubule minus end–binding protein, Patronin, colocalized with myosin and that actomyosin contractility organized microtubules in the medioapical cortex of apically constricting cells. We found that microtubules were required for mesoderm invagination, but not apical cortex contractility. Instead, proper microtubule organization promoted actomyosin attachment to adherens junctions. These results suggest that crosstalk between actomyosin and microtubules is critical for apical actomyosin attachments to adherens junctions and, thus, intercellular force transmission.

Results

Medioapical Patronin foci colocalize with myosin in apically constricting cells

To determine if the microtubule cytoskeleton plays a role in the invagination of mesoderm cells of the early *Drosophila* embryo, we first sought to establish the organization of the microtubule cytoskeleton. In most polarized epithelial cells, linear arrays of microtubules align with the apical–basal axis such that the minus ends are uniformly localized across the apical surface (Bacallao et al., 1989; Khanal et al., 2016; Toya et al., 2016). These minus ends are often capped and stabilized by a family of calmodulin-regulated spectrin-associated proteins (CAMSAPs; Patronin in *Drosophila*), which specifically bind to microtubule minus ends (Goodwin and Vale, 2010; Khanal et al., 2016; Noordstra et al., 2016; Toya et al., 2016). We imaged live and fixed *Drosophila* embryos expressing Patronin::GFP driven by the ubiquitin promoter (Ubi-p63E-Patronin::GFP, hereafter referred to as Patronin::GFP). During gastrulation, there was a striking difference in Patronin::GFP localization between mesoderm (apically constricting) and ectoderm cells (not constricting; Fig. 1 B). Specifically, Patronin::GFP was polarized to a central focus in the medioapical cell cortex of mesoderm cells but was enriched at cell junctions in the ectoderm (Fig. 1, B and C; and Video 1).

To demonstrate the difference in Patronin localization between these cell types, we measured the ratio of average junctional Patronin::GFP intensity to the average medial Patronin::GFP intensity. During mesoderm invagination, there was a significant difference in the ratio of junctional to medial Patronin::GFP intensity between mesoderm and ectoderm cells, with medial enrichment of Patronin::GFP intensity being highest in the mesoderm (mean junctional to medial ratio of 0.75 ± 0.53 compared with 4.75 ± 3.47; Fig. 1 D). In addition, the maximum medioapical Patronin::GFP intensity was higher in the mesoderm than the ectoderm, consistent with Patronin forming a large apical focus in these cells (Fig. 1 E). In contrast, Patronin::GFP in the ectoderm formed smaller puncta that were distributed across the apical cortex (Fig. 1 B).

Earlier in development, from syncytial to early cellularization stages, Patronin::GFP localized to the two centrosomes above the nucleus (Fig. 1 C). During mid to late cellularization, Patronin::GFP shifted to a more apical localization at cell junctions in both the mesoderm and ectoderm (Fig. 1 C and Video 1), consistent with another study at this developmental stage (Takeda et al., 2018). During gastrulation, medioapical Patronin::GFP foci localized to the center of medioapical myosin patches (Fig. 1 F). This localization mirrors that of active RhoA and ROCK (Mason et al., 2013, 2016). Interestingly, apical constriction of the posterior midgut cells (i.e., the endoderm) also exhibited medioapical Patronin::GFP enrichment (Fig. 1 G). These results demonstrated that medioapical Patronin localization is a fundamental organization shared by apically constricting cells during *Drosophila* gastrulation.

Medioapical Patronin stabilizes noncentrosomal microtubules

Given the striking and centralized Patronin::GFP localization in mesoderm cells, we next determined if this structure represented a centrosome or another type of microtubule-organizing center. First, we fixed embryos and detected α-Tubulin by immunofluorescence. When viewing cells en face, mesoderm cells displayed both punctate and fiber-like structures, suggesting that microtubules are arranged both parallel and perpendicular to the apical surface (Fig. 2, A and B). In contrast, the ectoderm had significantly fewer apical microtubules at the time of mesoderm invagination (Fig. 2 B). Because fixation often destroys dynamic cytoskeletal networks, we next visualized microtubules in live embryos expressing GFP-tagged CLIP170, a plus end–binding protein (Perez et al., 1999), which gave us the best labeling of microtubules at this stage. During early tissue folding, we observed dense patches of GFP::CLIP170 puncta that colocalized with apical myosin and Patronin (Fig. 2, C and D; and Video 2). Thus, these CLIP170-dense patches that colocalized with Patronin resembled apical microtubule-organizing centers. Consistent with this, at high temporal resolution, we observed GFP::CLIP170 comets, which suggested microtubule growth, moving from medioapical patches toward cell edges (Fig. 2, D and E). However, we also observed other directionalities in microtubule growth across the cell apex (Fig. 2 D).

Apical Patronin is often associated with noncentrosomal microtubules in epithelia (Noordstra et al., 2016; Toya et al., 2016). To test whether these Patronin foci were centrosomes, we examined the position of centrosomal markers, which were significantly below the apical surface throughout folding (Figs. 2 F and S1 A). We observed lower levels of Patronin::GFP associated with centrosomes, which were well separated from medioapical Patronin::GFP foci (Fig. 2 F). This localization could reflect sites of active Patronin-mediated minus end stabilization of microtubules that are released from centrosomes, similar to a proposed function of ninein (Mogensen et al., 2000; Moss et al., 2007), or a separate centrosomal pool of Patronin. Thus, there is a distinct organization of noncentrosomal microtubules at the apical cortex during mesoderm invagination.

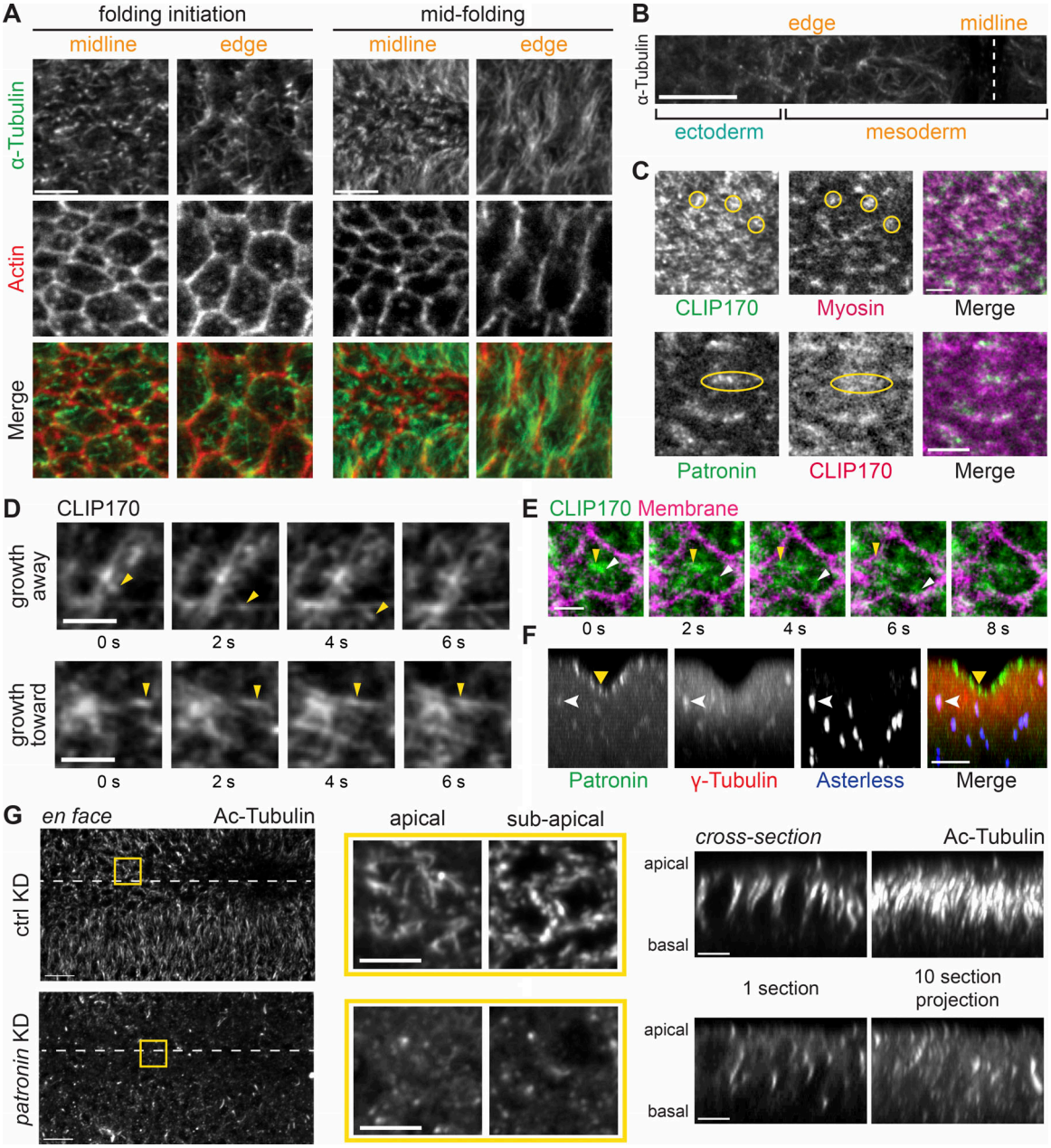

Figure 2. **Patronin stabilizes apical, noncentrosomal microtubules in the mesoderm. (A)** In the mesoderm, microtubules are oriented parallel and perpendicular to the apical membrane. Images are maximum-intensity projections from representative fixed embryos stained for α-tubulin (apical surface) and F-actin (subapical section, phalloidin). Surface views of cells along the midline and at the edge of the *snail*-expressing domain are shown for an embryo at folding initiation and midfolding. **(B)** Apical microtubules are enriched in mesoderm. Image is an apical surface Z-projection of a fixed embryo stained for α-tubulin. The furrow midline is marked with a dashed white line. **(C)** GFP::CLIP170 form dense clusters at the apical surface that colocalize with myosin (yellow circles; top) and Patronin (yellow ovals; bottom). Images are single apical sections from a live movie of an embryo expressing GFP::CLIP170 and Myo::mCH (sqh::mCH) or Patronin::GFP and CH::CLIP170. **(D)** Microtubule growth can be observed with dynamic GFP::CLIP170 comets (yellow arrowheads). Images are montages of single apical slices from representative live movies of embryos expressing GFP::CLIP170. **(E)** Microtubules grow from an apical microtubule-organizing center toward cell edges. Images are a montage of single apical slices from a live movie of an embryo expressing GFP::CLIP170 and Gap43::mCH. Different GFP::CLIP170 comets are marked with arrowheads. **(F)** Apical Patronin foci do not colocalize with centrosomal markers. Images are maximum-intensity projections of apical–basal cross sections from a representative fixed embryo stained for γ-tubulin (associated with centrosomes; Dictenberg et al., 1998; red), Asterless (Cep152, a centriolar component; Varmark et al., 2007; Dzhindzhev et al., 2010; blue), and endogenous Patronin::GFP signal (green). Medioapical Patronin (yellow arrowhead) is separate from Patronin::GFP signal at centrosomes (white arrowhead). **(G)** Depleting Patronin destabilizes microtubules. Images are apical surface projections of representative fixed embryos stained for acetylated-tubulin (Ac-Tubulin). The surface views of *rhodopsin-3* control RNAi (top) and *patronin*-RNAi knockdown (KD; bottom) are shown on the left. The ventral midline is marked by a white dashed line. Middle images are magnified en face views of apical and subapical projections in the yellow box. The right set of images show cross sections of the same embryos on the left. The left image is a single yz section, and the right image is a maximum-intensity projection of 10 cross sections. Scale bars represent 10 µm (B and G, tissue-wide view), 5 µm (A; C, top; F; and G, magnified view and cross section), and 3 µm (C, bottom; and D and E).

A well-known function of CAMSAPs is to stabilize microtubules (Goodwin and Vale, 2010; Tanaka et al., 2012; Hendershott and Vale, 2014; Jiang et al., 2014). To determine whether Patronin stabilizes noncentrosomal microtubules near the apical cortex, we fixed Patronin-depleted embryos and immunostained with antibodies against acetylated α-tubulin, a marker of stable microtubule polymers (Westermann and Weber, 2003). We verified that RNAi depleted Patronin protein levels by Western blot (Fig. S1 B). Control or wild-type embryos exhibited acetylated microtubules that were both lying across the apical surface and parallel to the apical–basal axis (Fig. 2 G). In contrast to controls, Patronin depletion dramatically reduced visible bundles of acetylated α-tubulin (eight out of eight embryos imaged; Fig. 2 G). When we examined microtubules in live embryos by imaging GFP::CLIP170, we observed that the organization of apical microtubules was disrupted in Patronin-depleted embryos during gastrulation, with centrosomes abnormally localized close to the apical surface (five out of five embryos imaged; Fig. S1 C). This result suggested that Patronin stabilizes apical, noncentrosomal microtubules and promotes their organization.

Finally, to determine whether Patronin localization required microtubules, we injected Patronin::GFP-expressing embryos with the microtubule depolymerizing drug colchicine. Colchicine injection dramatically disrupted Patronin localization (Fig. S1 D), consistent with the reported loss of polarized CAMSAP3 localization in Caco-2 cells treated with nocodazole, another inhibitor of microtubule polymerization (Toya et al., 2016). Together, these results suggested that medioapical Patronin foci form a noncentrosomal microtubule-organizing center in constricting mesoderm cells and that Patronin and microtubule localization is interdependent.

Patronin puncta coalesce into foci during myosin pulses

During mesoderm invagination, apical myosin initially accumulates in cycles of assembly and disassembly, and these pulses are associated with apical constriction (Martin et al., 2009; Vasquez et al., 2014). To determine how medioapical Patronin foci form, we analyzed the spatiotemporal dynamics of Patronin::GFP relative to myosin. In contrast to myosin, we did not observe clear cycles of assembly and disassembly for Patronin::GFP puncta (Fig. 3 A and Video 3). Instead, medioapical Patronin foci appeared to grow by the continuous coalescence of smaller Patronin::GFP puncta (Fig. 3 A). To determine if Patronin::GFP coalescence was associated with apical myosin contraction, we identified individual myosin pulses and analyzed the behavior of Patronin::GFP in the region of the pulse. During myosin pulse assembly, we usually observed instances of Patronin::GFP coalescence, which formed a brighter, more compact focus (Fig. 3 B). When we analyzed the maximum-intensity profiles of myosin and Patronin::GFP averaged across 20 pulses, we found that myosin intensity peaked ∼5 s before maximum Patronin::GFP intensity (Fig. 3 C). These data suggested that actomyosin pulses form medioapical Patronin foci, which we showed colocalize with apical myosin patches (Fig. 1 F).

During myosin pulse disassembly, there were local decreases in Patronin::GFP intensity as more compact Patronin foci sometimes appeared to relax and revert back to separate, smaller puncta (Fig. 3, C and D). To determine how closely changes in Patronin intensity tracked with myosin intensity, we analyzed the time-resolved cross-correlation between changes in Patronin::GFP and myosin intensities. We identified a significant correlation that occurred between these two signals, with the maximum correlation occurring at a time offset of −3.9 s, consistent with increases in myosin signal preceding increases in Patronin signal (Fig. 3 E). These results demonstrated a tight correlation between myosin and Patronin intensity, with myosin preceding Patronin coalescence, suggesting that actomyosin contraction forms medioapical Patronin foci in mesoderm cells, possibly through an advection-based mechanism (Munro et al., 2004; Munjal et al., 2015).

Actomyosin contraction forms a medioapical, noncentrosomal microtubule-organizing center

Because microtubule/Patronin organization in the mesoderm resembled that of active RhoA and was correlated with myosin contractility (Fig. 3; Mason et al., 2013, 2016), we tested whether RhoA and actomyosin contractility were required to organize apical noncentrosomal microtubules. Because ROCK is the main myosin kinase in early *Drosophila* embryos, we injected embryos with the ROCK inhibitor Y-27632 (Royou et al., 2002; Dawes-Hoang et al., 2005). In comparison to water-injected embryos, Y-27632 disrupted Patronin::GFP apical localization (Fig. 4, A and B). However, because Y-27632 also inhibits atypical PKC (Davies et al., 2000), we additionally analyzed Patronin localization after inhibiting RhoA activity with the C3 exoenzyme (Crawford et al., 1998). RhoA inhibition similarly disrupted apical Patronin (Fig. 4, C and D), suggesting that RhoA activity promotes the formation of a medioapical microtubule-organizing center.

Because RhoA also promotes contraction via F-actin assembly (Evangelista et al., 1997; Watanabe et al., 1997; Grosshans et al., 2005; Otomo et al., 2005; Fox and Peifer, 2007; Murrell et al., 2015; Agarwal and Zaidel-Bar, 2019), we tested whether disrupting the apical F-actin network affects microtubule organization by injecting drugs that interfere with F-actin assembly, such as cytochalasin D (CytoD) and latrunculin B (LatB). Similar to Y-27632 and C3 exoenzyme injections, both CytoD and LatB disrupted medioapical Patronin foci formation. In these embryos, Patronin puncta did not coalesce and remained as small, dynamic puncta (Figs. 4 E and S2 A). Importantly, it has been shown in Caco-2 cells, where CAMSAP3 localizes as puncta in the apical cortex, that F-actin depolymerization reduces CAMSAP3 puncta in cortical regions (Toya et al., 2016). Many of these smaller Patronin puncta colocalized with myosin, suggesting physical association between the two cytoskeletal networks (Fig. S2 B). Altogether, our data indicated that RhoA activity, which leads to actomyosin contraction, is required to organize apical, noncentrosomal microtubules during mesoderm invagination.

During *Drosophila* gastrulation, RhoA activity at the apical surface in apically constricting cells is downstream of G-protein-coupled receptor signaling that is activated by the extracellular ligand, Folded gastrulation (Fog; Costa et al., 1994; Dawes-Hoang et al., 2005). Thus, we tested whether Fog signaling was

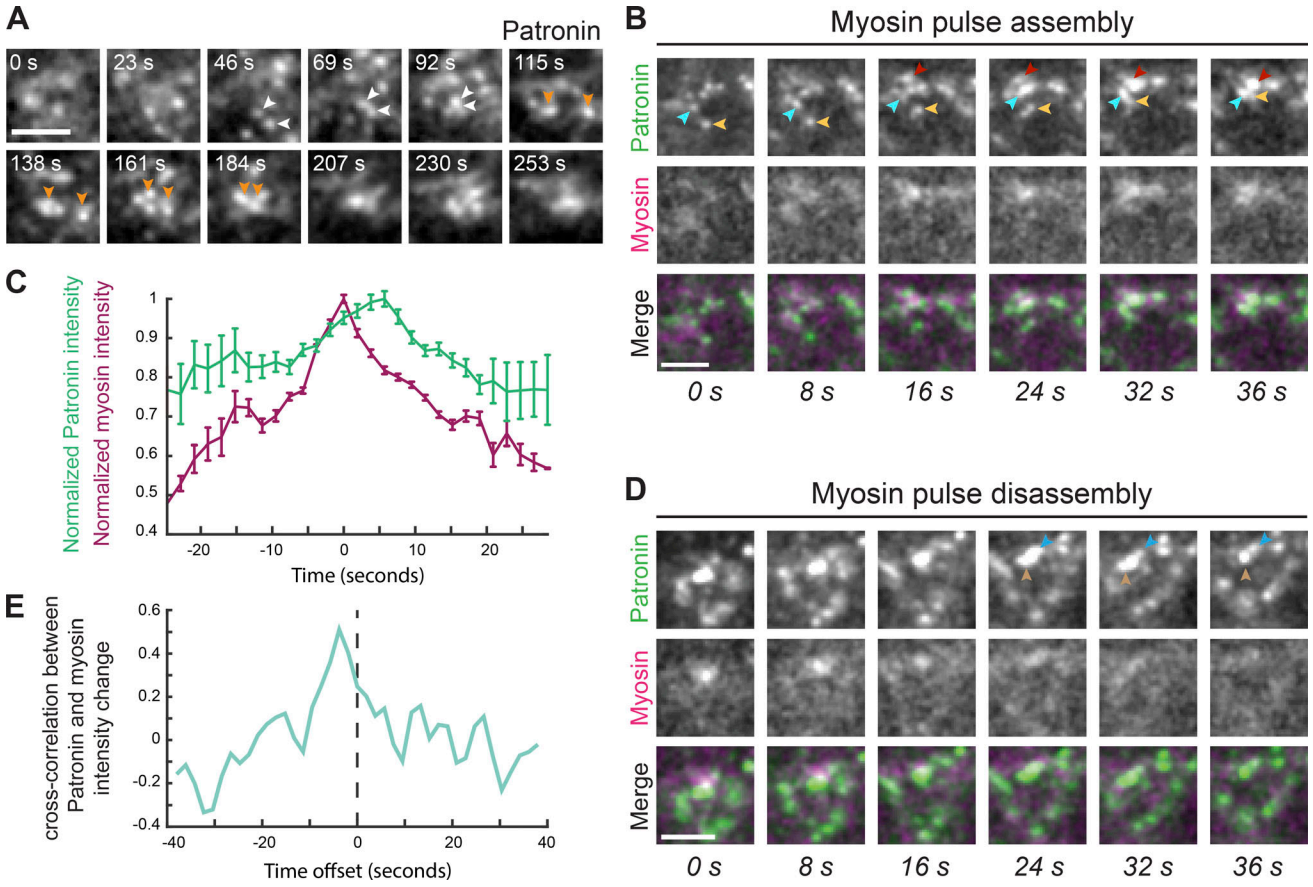

Figure 3. **Medioapical Patronin foci form by coalescence during myosin assembly. (A)** Patronin foci form by coalescence of smaller puncta (arrowheads). Time-lapse images are from single apical sections from a live movie of a representative embryo expressing Patronin::GFP. **(B)** Patronin puncta coalescence (arrowheads) occurs during myosin pulse assembly. Time-lapse images represent a myosin pulse (single apical slice) from a live movie of an embryo expressing Patronin::GFP and Myo::mCH. **(C)** Quantification of average maximum Myo::mCH and Patronin::GFP intensity (n = 4 embryos, 5 pulses per embryo) after normalizing and aligning the maxima of Myo::mCH across all 20 pulses. Time at peak mean myosin intensity was centered at 0. Error bars represent the standard error of the mean. **(D)** During myosin pulse disassembly, local Patronin::GFP intensity decreases and larger foci revert back to smaller puncta (arrowheads). Time-lapse images are a representative pulse from a single apical section from a live movie of an embryo expressing Patronin::GFP and Myo::mCH. **(E)** Myosin and Patronin intensity are tightly correlated. Plotted is the mean time-resolved correlation function between changes in Myo::mCH and Patronin::GFP intensity. Maximum correlation occurs at an offset of approximately −4 s. Dashed line indicates time offset of 0 s. Scale bars represent 3 µm.

sufficient to organize apical, noncentrosomal microtubules. Ectopic Fog expression outside the mesoderm leads to apical myosin activation across the entire surface of the embryo (Dawes-Hoang et al., 2005). When we looked at Patronin::GFP localization in ectodermal tissues in embryos overexpressing Fog, we observed medioapical foci of Patronin::GFP (10/10 embryos imaged), in contrast to the largely junctional localization of Patronin::GFP in control embryos, as described above (Fig. 1, B and D; and Fig. 4 F). Therefore, our data supported the hypothesis that RhoA and actomyosin contractility, downstream of Fog signaling, drive the formation of apical, noncentrosomal microtubule-organizing centers.

Microtubules are not required for initiating apical contractility or adherens junction assembly

Studies in other developmental contexts have shown that microtubules are necessary for cell invagination (Lee et al., 2007; Booth et al., 2014). Consistent with this, we found that microtubules were also important for mesoderm cell invagination (Fig. 5 A and Video 4). Given the striking organization of the microtubule cytoskeleton in the mesoderm, we sought to determine how microtubules promote cell invagination. For example, microtubules could help induce contractility, such as by activating apical actomyosin assembly (Rogers et al., 2004; Booth et al., 2014). Another possibility is that microtubules could regulate adherens junction assembly or position to promote cell adhesion and/or force transmission (Harris and Peifer, 2005; Stehbens et al., 2006; Meng et al., 2008; Le Droguen et al., 2015). Furthermore, microtubules might regulate the connection between actomyosin networks and the adherens junctions.

To determine whether microtubules are required to initiate contractility in mesoderm cells, we disrupted microtubules pharmacologically or by gene depletion. Embryos staged at late cellularization were acutely injected with drugs that disrupt the microtubule cytoskeleton and were imaged within minutes after injection. Despite tissue folding failure, we found that colchicine injection did not disrupt apical myosin activation or the initiation of apical constriction (19/19 embryos imaged; Fig. 5 A and

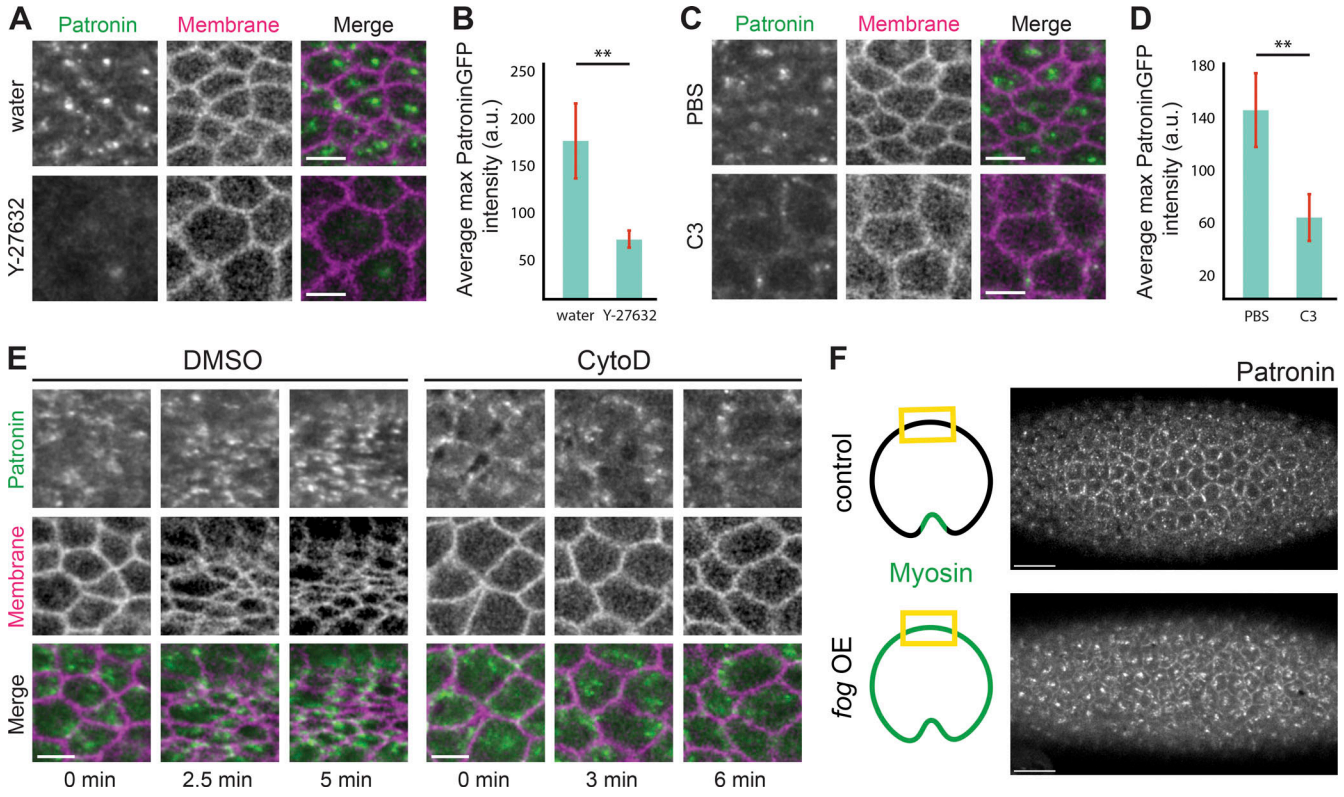

Figure 4. **Medioapical Patronin foci depend on actomyosin contraction. (A)** ROCK inhibitor disrupts apical Patronin localization in the mesoderm. Images are maximum-intensity Z-projections of mesoderm cells from representative live embryos expressing Patronin::GFP (apical surface) and Gap43::mCH (subapical section) injected with water (top) or Y-27632 (50 mM; bottom). **(B)** ROCK inhibitor decreases Patronin::GFP apical intensity. Quantification of average maximum Patronin::GFP intensity in a region that spans the apical cortex (n = 7 measurements per embryo, four embryos per condition; **, P < 0.0001, unpaired t test). Error bars represent one standard deviation. **(C)** RhoA inhibition disrupts medioapical Patronin localization. Images are maximum-intensity Z-projections from representative live embryos expressing Patronin::GFP (apical surface) and Gap43::mCH (subapical section) injected with PBS (top) or the C3 exoenzyme (1 mg/ml; bottom). **(D)** RhoA inhibition decreases apical Patronin::GFP intensity. Quantification of average maximum Patronin::GFP intensity in a region that spans the apical cortex (n = 7 measurements per embryo, four embryos per condition; **, P < 0.0001, unpaired t test). Error bars represent one standard deviation. **(E)** Disrupting the apical F-actin network disrupts medioapical Patronin foci formation. Time-lapse images are maximum-intensity Z-projections from live embryos expressing Patronin::GFP (apical surface) and Gap43::mCH (subapical section) injected with DMSO (left) and CytoD (0.125 mg/ml; right). **(F)** fog signaling is sufficient to form ectopic medioapical Patronin foci in the ectoderm. Images are maximum-intensity projections of control and *fog*-overexpressed embryos expressing Patronin::GFP. The tissue regions shown in the images are highlighted by yellow boxes in the cartoon diagrams. Scale bars represent 15 µm (F) and 5 µm (A–E).

Video 4). To demonstrate that apical constriction occurred, we measured apical area at the onset of constriction and ∼5 min later for both control and drug-injected embryos (Fig. 5 B). Depleting Patronin by RNAi also disrupted tissue folding (11/44 embryos imaged) without affecting mesoderm cell fate, apical myosin localization, or constriction onset (44/44 embryos imaged; Fig. S3, A–C). Interestingly, Patronin depletion caused an initial heterogeneity in apical cell area (44/44 embryos imaged; Fig. S3 A), consistent with prior observations in *Drosophila* embryos (Takeda et al., 2018).

To test whether microtubule dynamics/organization were important for apical force generation, we injected embryos with Taxol, a microtubule-stabilizing agent. Taxol injection disrupted apical microtubule organization, resulting in thick bundles that spanned the apical surface (Fig. S3 D). Perturbing microtubule dynamics/organization with Taxol disrupted folding but had no effect on initial cell constrictions or myosin accumulation (21/21 embryos imaged; Fig. 5, B and C). Furthermore, Taxol-injected embryos exhibited a clear cross-correlation peak between apical constriction rate and the rate of change in myosin intensity, which is indicative of normal myosin pulsing (Fig. 5 D; Mason et al., 2013; Vasquez et al., 2014). Finally, the apically polarized localization of ROCK was unaffected in both colchicine- and Taxol-injected embryos (Fig. 5 E). These data suggested that microtubule organization is not important for apical actomyosin activation and the subsequent onset of apical constriction.

To determine if microtubules were required for apical adherens junction assembly (Dawes-Hoang et al., 2005; Stehbens et al., 2006; Kölsch et al., 2007; Marston et al., 2016; Weng and Wieschaus, 2016), we analyzed E-cadherin in live embryos injected with microtubule drugs or depleted of Patronin. There were no gross defects in apical E-cadherin structure or polarity in either case (Fig. 5 F and Fig. S3, B and C). We measured raw intensity values of E-cadherin::GFP at the onset of constriction and calculated the average ratio of junctional to medial E-cadherin::GFP intensity in DMSO-, colchicine-, and Taxol-injected embryos. In all cases, E-cadherin was present and junctionally enriched (Fig. 5 G). Consistent with proper adherens junction

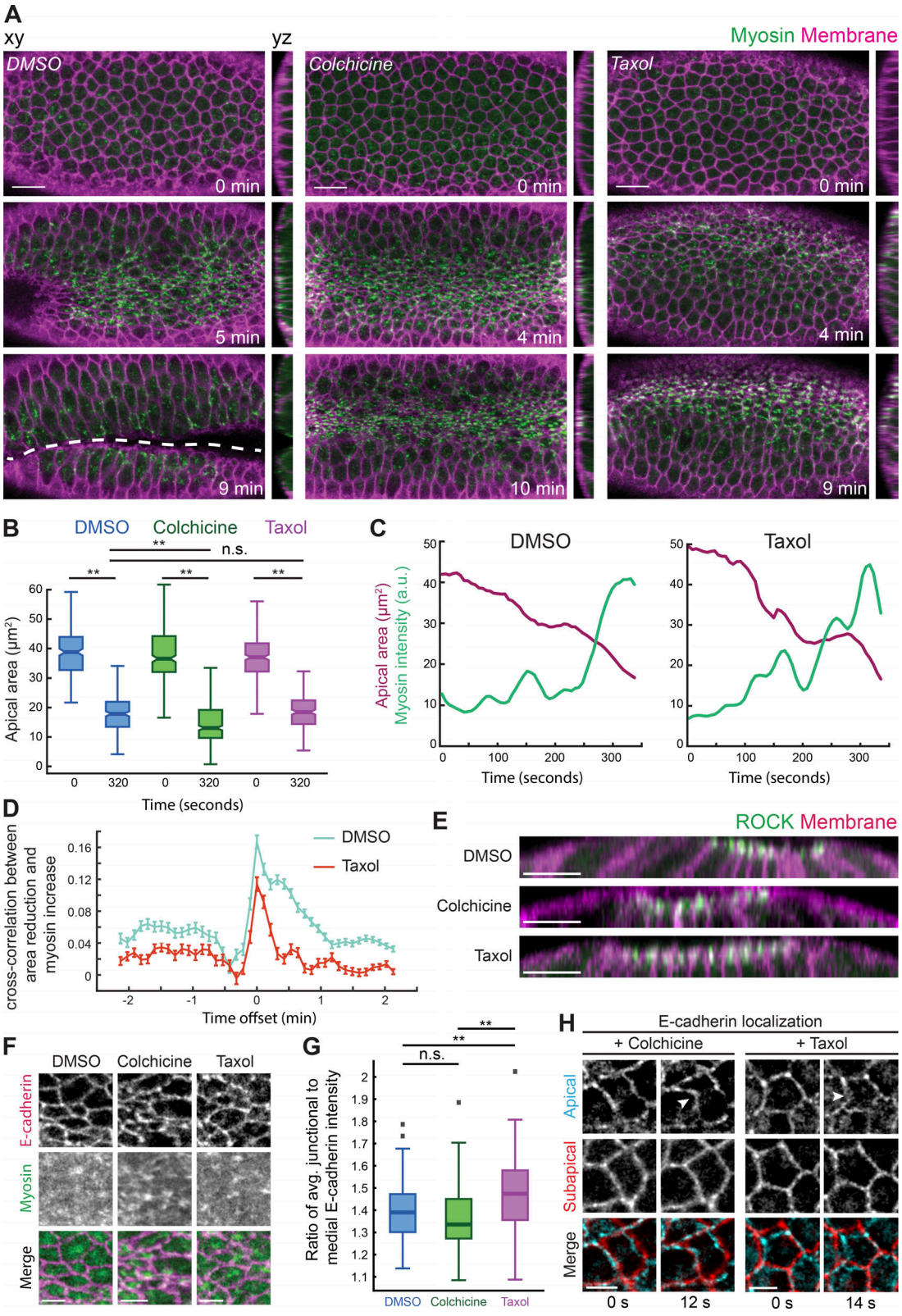

Figure 5. **Apical myosin activation and apical constriction initiation do not require microtubules. (A)** Disrupting microtubules prevents folding, despite apical myosin activation and apical constriction initiation. Time-lapse images are maximum-intensity Z-projections from representative live embryos expressing Myo::GFP (apical surface) and Gap43::mCH (membrane, subapical section) injected with DMSO (left), colchicine (5 mg/ml; middle), and Taxol (5 mg/ml; right). Apical–basal cross sections (yz) are to the right of each image. Dashed line indicates the ventral furrow. **(B)** Apical area initiates reduction after disrupting microtubules. Quantification of apical cell areas preconstriction (t = 0 s) and 320 s after from three representative live embryos injected with DMSO (n = 226 cells, T = 0 s; 252 cells, T = 320 s; **, P < 0.0001, unpaired t test), colchicine (n = 284 cells, T = 0 s; 353 cells, T = 320 s; **, P < 0.0001, unpaired t test),

and Taxol (n = 275 cells, T = 0 s; 226 cells, T = 320 s; **, P < 0.0001, unpaired t test). The notch is the median, and bottom and top edges of the box are the 25th and 75th percentiles; whiskers extend to the most extreme data points. **(C)** Myosin assembly and pulses still occur after inhibiting microtubule dynamics. Graphs show apical area and myosin intensity over time in representative single cells in DMSO- (top) and Taxol-injected (bottom) embryos. **(D)** Disrupting microtubule dynamics does not initially interfere with the correlation between myosin increase and area reduction. Plotted is the mean time-resolved correlation function between constriction rate (positive constriction = area decrease) and myosin rate. Data are from three representative embryos injected with DMSO (n = 548 cells) or Taxol (n = 543 cells). Error bars represent the standard error of the mean. **(E)** Microtubule disruption does not affect apical ROCK polarity. Images show apical–basal cross sections from representative live embryos expressing ROCK::GFP and Gap43mCH injected with DMSO, colchicine, or Taxol. **(F)** Apical spot adherens junctions are unaffected by microtubules disruption. Images are apical surface projections of representative live embryos expressing E-cadherin::GFP and Myo::mCH injected with DMSO (left), colchicine (middle), and Taxol (right). **(G)** Quantification of junctional E-cadherin enrichment. Individual cells at the onset of constriction were segmented and the ratio of average raw junctional to medioapical E-cadherin::GFP intensity was calculated for two or three representative DMSO- (n = 122 cells), colchicine- (n = 67 cells), and Taxol-injected (n = 105) embryos (**, P < 0.0001, unpaired t test). Bottom and top edges of the box are the 25th and 75th percentiles, and whiskers extend to the most extreme data points; outliers are included (gray squares). **(H)** Apical spot junctions are pulled in during initial cell constrictions after microtubule disruption. Time-lapse images showing a single apical (cyan) and subapical (red) slice of representative embryos expressing E-cadherin::GFP injected with colchicine (left) and Taxol (right). Arrowheads point to an apical spot junction that has been pulled inwards in the second frame. Scale bars represent 15 µm (A), 10 µm (E), and 5 µm (F–H).

assembly, we observed wavy and deformed cell–cell interfaces at the apical surface, which suggested that medial actomyosin was initially able to pull on spot adherens junctions (Fig. 5 H). Thus, during mesoderm invagination, microtubules are not necessary to initiate contractility (i.e., apical myosin activation) or assemble apical adherens junctions but are still required for tissue folding.

Proper microtubule organization promotes intercellular force transmission

In the previous section, we showed that initiation of apical myosin and adherens junction accumulation was largely unaffected in Patronin-depleted and colchicine- and Taxol-injected embryos. Another possibility was that microtubules promote the connection between actomyosin and adherens junctions and/or promote reattachment of lost connections (Roh-Johnson et al., 2012; Jodoin et al., 2015). Therefore, we analyzed actomyosin attachments to adherens junctions and the resulting intercellular connectivity between actomyosin networks after microtubule cytoskeleton disruption. In both colchicine- and Taxol-injected embryos, apical myosin networks exhibited striking separations well after apical constriction onset (Fig. 6, A and B; Fig. S4 A; and Video 5). Myosin spots in different cells chaotically separated and then moved back together and the apex of cells became distended, losing their constricted morphologies (Figs. 6 B and S4 A and Video 5). The loss of intercellular connectivity of actomyosin after microtubule disruption was not associated with a fracture of the medioapical ROCK/myosin signaling center, because embryos expressing GFP-tagged ROCK injected with Taxol exhibited ROCK/myosin foci that clearly separated from the junctional domain (Fig. S4 B). The phenotypes were not caused by disrupting a previous developmental process, such as cellularization, because injecting colchicine into live embryos that had completed cellularization and started apical constriction (i.e., injected when apical myosin was present) resulted in the same phenotype (two out of two embryos imaged; Fig. S4 C). Thus, microtubules are required during tissue folding to maintain actomyosin attachments to adherens junctions.

When we perturbed microtubules by depleting Patronin by RNAi, which we showed destabilized apical noncentrosomal microtubules and disrupted their organization (Figs. 2 G and S1 C), we also observed dynamic tearing of the myosin network in 11 out of 44 knockdowns (Fig. 6 C). We believe that the lower penetrance of the *patronin*-RNAi treatment reflects the less severe effect of Patronin depletion on microtubule organization. In both drug-injected and Patronin-depleted embryos, these separations only occurred after a significant buildup of apical myosin and the initial formation of a supracellular myosin network, suggesting that microtubules are important at later stages of the folding process when cells must stabilize their shape in the face of significant tension.

To determine how actomyosin network structures separated from each other, we examined the F-actin cortex using a GFP-tagged F-actin–binding domain of Utrophin (Utr::GFP; Rauzi et al., 2010). Similar to wild-type embryos (Jodoin et al., 2015), DMSO-injected embryos exhibited a dynamic F-actin cortex where apical F-actin holes that appeared next to intercellular junctions were rapidly repaired, usually within ∼20–60 s (Fig. 6, D and E). In contrast, Taxol-injected embryos exhibited longer-lived holes or fractures in the F-actin meshwork, and these fractures often grew larger to encompass multiple neighboring cells (Fig. 6, D and E; and Video 6). These results suggested that actomyosin network separations occur due to the separation of the apical F-actin meshwork from intercellular junctions (Fig. 6, D–F). We previously showed that E-cadherin was still present at junctions after microtubule disruption (Fig. 5, F–H; and Fig. S3, B and C). To determine whether the actomyosin cortex separates from adherens junctions, we visualized E-cadherin and found that E-cadherin persists at the cell–cell interface between myosin separations (Fig. 6 B). Moreover, actomyosin network separations were repaired as myosin in neighboring cells reestablished connections and pulled back together (Figs. 6 B and S4 A and Video 5), which further suggested the presence of functional adherens junctions. Only at much later stages, when tissue integrity was completely lost, did we observe E-cadherin mislocalized across the apical cortex (Fig. S4 D).

Because actin turnover reattaches the F-actin cortex to junctions (Jodoin et al., 2015), the greater persistence of the F-actin holes after microtubule disruption suggested that microtubules could promote force transmission by inducing actin turnover. We examined whether microtubules influenced the localization of known F-actin–binding proteins that localize to junctions. We fixed embryos minutes after either DMSO or

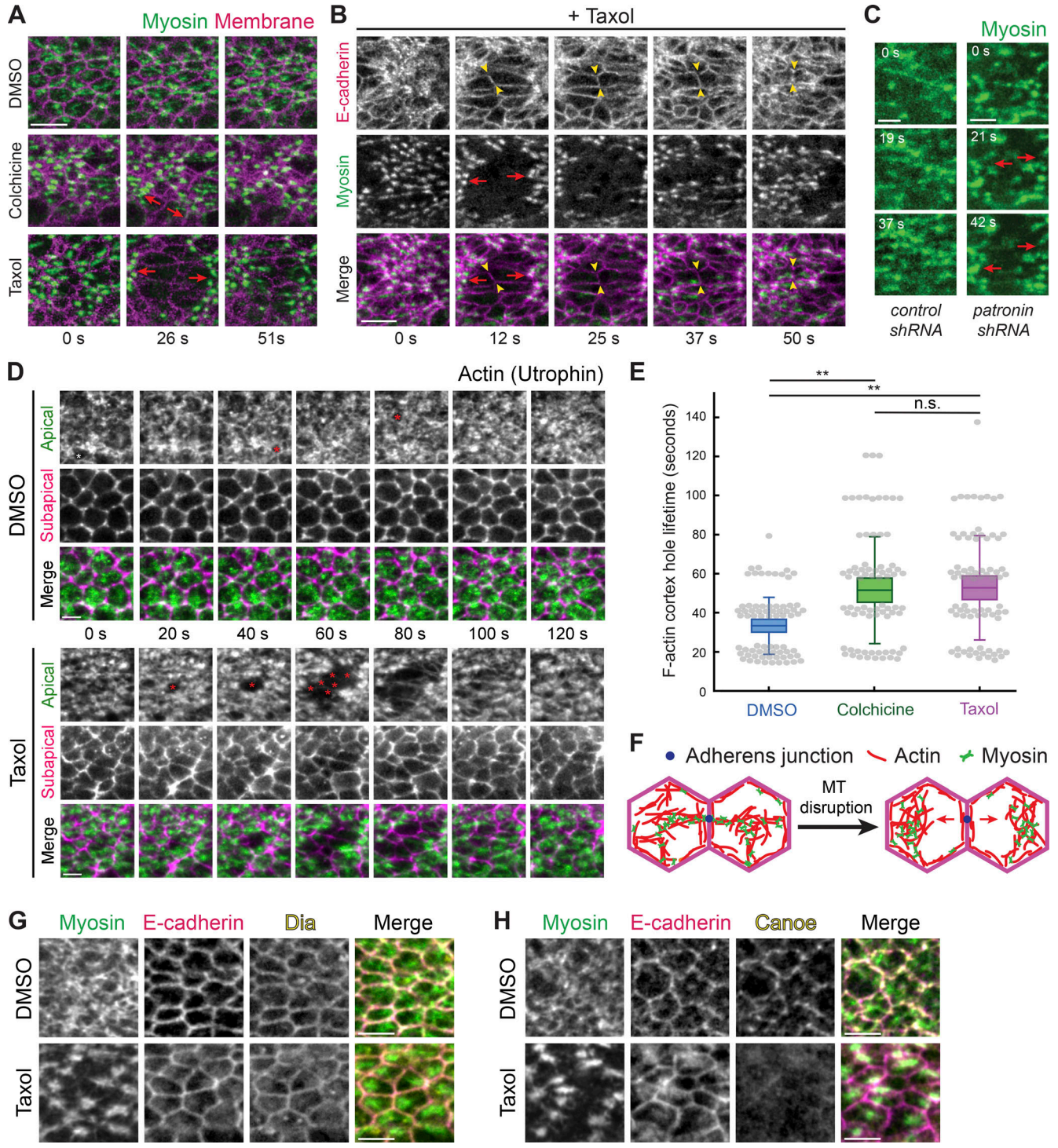

Figure 6. **Microtubules stabilize actomyosin connections to intercellular junctions. (A)** Microtubule disruption leads to separations between myosin structures and intercellular junctions. Time-lapse images are maximum-intensity Z-projections from live embryos expressing Myo::GFP (apical surface) and Gap43::mCH (subapical section illustrating junctions) injected with DMSO (top), colchicine (5 mg/ml; middle), and Taxol (5 mg/ml; bottom). Red arrows indicate the direction in which myosin structures separate from cell junctions. **(B)** E-cadherin is still present at interfaces between myosin spot separations. Time-lapse images are maximum-intensity Z-projections of apical Myo::mCH and an apical Z-slice of E-cadherin::GFP for a representative embryo injected with Taxol (5 mg/ml). Red arrows indicate the direction in which myosin spots separate from cell junctions. One cell–cell interface is highlighted between arrowheads. **(C)** Depleting Patronin also causes myosin network separation. Time-lapse images are apical projections from representative live embryos expressing Myo::GFP and shRNA against *rhodopsin-3* (control, top) and *patronin* (bottom). Arrows indicate the direction in which myosin spots separate from cell junctions. **(D)** Taxol injection causes longer-lived and larger holes in the F-actin cortex (asterisks), which leads to separation of F-actin meshworks away from junctions. Time-lapse images are maximum-intensity Z-projections of apical slices (green) and a subapical slice (magenta) from representative live embryos expressing Utr::GFP injected with DMSO or Taxol (5 mg/ml). **(E)** The lifetime of holes in the F-actin cortex near cell junctions is longer when microtubules are disrupted. Quantification of hole lifetime length at a resolution of ∼20 s between time steps for 75 holes across three embryos in each condition (**, P < 0.0001, unpaired

t test). Bottom and top edges of the box are the 25th and 75th percentiles, and whiskers extend to the most extreme data points, excluding outliers. All data points were plotted as gray dots. **(F)** Diagram showing a model of myosin separation. Shown is a top down view of the apical cortex in two adjacent cells. Loss of attachment of actomyosin to the adherens junction (blue dot) after microtubule (MT) disruption leads to actomyosin network separation. **(G)** Microtubule disruption does not affect junctional localization of Dia. Images are from representative embryos expressing Myo::GFP that were injected with DMSO (left) or Taxol (5 mg/ml; right), PFA fixed, and immunostained with antibodies against E-cadherin and Dia. **(H)** Microtubule disruption affects junctional localization of Cno. Images are from representative embryos expressing Myo::GFP that were injected with DMSO (left) or Taxol (5 mg/ml; right), PFA fixed, and immunostained with antibodies against E-cadherin and Cno. Scale bars represent 10 µm (A and B) and 5 µm (C–H).

Taxol injection and stained for the formin Diaphanous (Dia), which is enriched at junctions (Mason et al., 2013), and Canoe (Cno), the *Drosophila* Afadin homologue that mediates linkages between F-actin and adherens junctions (Sawyer et al., 2009; Choi et al., 2016). In both conditions, we observed a clear junctional enrichment of Dia (five out of five DMSO embryos and six out of six Taxol embryos; Fig. 6 G). However, we cannot rule out that microtubules promote Dia activity, as CLIP170 has been shown to stimulate mDia1 activity (Henty-Ridilla et al., 2016). In contrast, we observed a striking loss of junctional Cno localization after Taxol injection (four out of four DMSO embryos and four out of four Taxol embryos; Fig. 6 H). These results suggested that proper microtubule organization is required for Cno localization at adherens junctions, which could promote F-actin recruitment and linkage to the adherens junction (see Discussion). Overall, our results demonstrated that microtubules are critical for actomyosin networks in adjacent cells to stably transmit force to each other across adherens junctions by promoting reattachment of apical actin meshworks to the junctions (Fig. 6 F).

Discussion

Our work identifies a role for microtubules in promoting force transmission between epithelial cells during *Drosophila* mesoderm invagination. We have demonstrated, to our knowledge, a novel organization to the microtubule cytoskeleton, where a medioapical focus of the microtubule minus end–binding protein Patronin is present in apically constricting cells. Patronin puncta coalesce to form medioapical Patronin foci, which depends on actomyosin contraction. Patronin stabilizes and organizes apical, noncentrosomal microtubules, which grow from this center to intercellular junctions. Microtubules are dispensable for apical myosin polarity, apical E-cadherin, and initiation of apical constriction but are required to promote medioapical actomyosin network attachment to E-cadherin–based cell junctions. Disrupting microtubules results in dynamic separations between myosin and intercellular junctions at later stages of tissue folding that prevent mesoderm invagination. This study uncovers a previously unrecognized role for microtubule organization in integrating contractile forces across a tissue during morphogenesis, possibly by regulating actin turnover.

Apical constriction in the early *Drosophila* embryo is associated with a medioapical, noncentrosomal microtubule-organizing center

Apically constricting cells in the mesoderm and endoderm shared a similarly polarized microtubule organization with Patronin foci localized to the medioapical cortex. In addition, live imaging of embryos expressing GFP::CLIP170 revealed the appearance of dense patches of microtubules in the mesoderm that colocalized with both apical myosin patches and Patronin foci. Microtubules were observed to grow from medioapical patches toward cell junctions. Given the high concentration of microtubule-associated proteins that localize to the medioapical focus, this resembles a type of noncentrosomal microtubule-organizing center. It is unclear how similar this noncentrosomal microtubule organization is to the organization that has been observed for centrosomal microtubules in MCF-7, MDCK, and hE-CHO cells (Stehbens et al., 2006), where microtubules radiate out from centrosomes with growing plus ends enriched toward cell edges. However, in support of this view, both fixed and live data suggested that microtubules span the apical cortex and we observed CLIP170 puncta at cell junctions. Together, these results suggest that the medioapical cortex is a zone of microtubule minus end stabilization that could act as an organizing center from which microtubules grow toward cell junctions (Fig. 7 A).

Patronin foci colocalized with apical myosin patches and formed by coalescence that spatiotemporally correlated with myosin pulses. During myosin pulses, peak Patronin intensity was observed ∼5 s after peak myosin intensity. Thus, polarized Patronin organization may be a consequence of medioapical actomyosin contraction. Consistent with this, overexpressing Fog, whose expression is normally restricted to ventral cells by the mesoderm-specific transcription factor Twist (Costa et al., 1994; Kölsch et al., 2007), was sufficient to reorganize microtubules in ectopic tissues. Thus, Patronin, which is maternally deposited (Khanal et al., 2016; Nashchekin et al., 2016), exhibits tissue type–specific organization as a result of actomyosin contractility that is activated in the mesoderm and endoderm by Fog signaling, downstream of embryonic transcription factor expression. Furthermore, injecting higher doses of CytoD/LatB, which leads to the formation of small myosin and ROCK puncta that fail to coalesce (Mason et al., 2013; Coravos and Martin, 2016), caused Patronin to remain as small puncta that do not coalesce (Fig. 7 A). One possible connection between Patronin and F-actin is the spectrin cytoskeleton because spectrin associates with F-actin and Patronin has been shown to associate with spectrin isoforms (King et al., 2014; Khanal et al., 2016). However, Patronin's central localization also depends on microtubules, and it is possible that microtubules trapped in the actin network are "collected" by actomyosin contractile flow through advection (Salmon et al., 2002; Munro et al., 2004; Munjal et al., 2015). To our knowledge, this is the first example of actomyosin contraction forming a microtubule-organizing center.

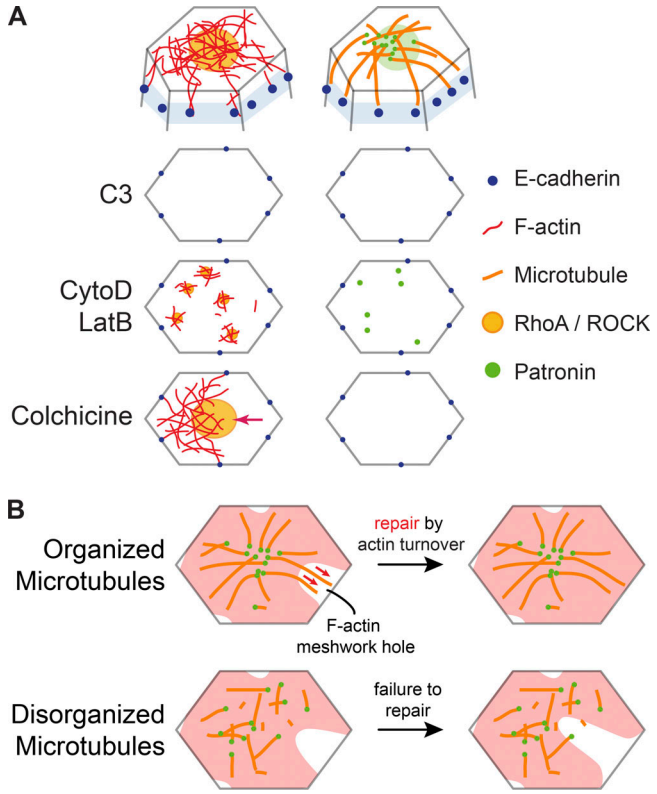

Figure 7. **Actin and microtubule cytoskeletons interact to promote intercellular force transmission. (A)** Diagrams at top show the proposed organization of the microtubule and actin cytoskeletal networks at the cell apex. Diagrams below show top down views of the apical cortex (without microtubules) and the effect of various perturbations on Rho/ROCK/F-actin and Patronin localization. C3 injection eliminates apical RhoA/ROCK and Patronin foci. CytoD/LatB injections lead to formation of smaller RhoA/ROCK and Patronin puncta. Colchicine injection does not affect RhoA/ROCK polarity but leads to actomyosin network separations from intercellular junctions (arrow). **(B)** A model for how microtubules promote reattachment of the apical F-actin meshwork to adherens junctions after fracture. In wild-type embryos (top), the organization of apical, noncentrosomal microtubules could promote repair of holes in the F-actin meshwork (red) by guiding F-actin polymerization and/or bundling through physical associations (red arrows). When microtubule organization is disrupted (bottom), the hole in the F-actin meshwork cannot be repaired in a timely manner, leading to actomyosin network separation from adherens junctions.

Additionally, separate from the microtubules that were localized at the apical cortex, we also observed clear arrays and bundles of microtubules along the apical–basal axis (Harris and Peifer, 2007). The interplay between apical–basal microtubule bundles near cell boundaries and the microtubule network at the apical cortex is still unclear. Apical–basal microtubule bundles may integrate with apical, noncentrosomal microtubules or behave as a separate microtubule population that has distinct functions during cell shape change and tissue invagination.

Microtubules are not required to initiate apical constriction in mesoderm cells

Apical constriction and subsequent tissue invagination have been shown to depend on microtubules in bottle cells during *Xenopus laevis* gastrulation and placodal cells during salivary gland tubulogenesis in *Drosophila* larvae (Lee and Harland, 2007; Booth et al., 2014). In the developing salivary gland cells, microtubules were required for the formation of a medioapical actomyosin network that constricted the cell apex (Booth et al., 2014), consistent with a proposed model for microtubule-dependent activation of RhoA at the apical cortex (Rogers et al., 2004). Apical cortex organization leading to polarized domains of active contractility is important during apical constriction (Mason et al., 2013; Booth et al., 2014; Coravos and Martin, 2016). However, in mesoderm cells during *Drosophila* gastrulation, depolymerizing microtubules or disrupting microtubule dynamics/organization did not lead to a loss of apical myosin activation and initiation of apical constriction was normal. Moreover, medioapical ROCK polarity was unaffected after Taxol injection. Overall, these data suggest that during mesoderm invagination in the early embryo, medioapical RhoA activity is not affected by microtubule perturbation. However, RhoA activity was important for microtubule organization (Fig. 7 A). Our work suggests that microtubules can affect apical constriction in other ways, such as by promoting actin network reattachment to the adherens junction after it fractures.

Microtubules promote actomyosin reattachment to adherens junctions

The earliest gastrulation phenotype we observed after disrupting microtubules was fracture occurring between apical actomyosin networks and adherens junctions, which failed to be repaired in a timely manner (Fig. 7 B). These apical actin cortex fractures led to the separation of myosin structures and persistent holes in the apical F-actin cortex, which were similar to phenotypes observed in embryos with disrupted actin turnover (Jodoin et al., 2015). Apical microtubules could promote adherens junction reattachment by promoting actin assembly around the adherens junction (Henty-Ridilla et al., 2016) or by promoting F-actin bundling around the adherens junction (López et al., 2014; Michael et al., 2016). These interactions may play a role in repairing F-actin meshwork holes to promote reattachment (Jodoin et al., 2015; Fig. 7 B). In addition, microtubules may promote actomyosin attachment to adherens junctions by physically associating with the apical F-actin network. Such an association could be mediated by actin-microtubule cross-linkers (Applewhite et al., 2010; Girdler et al., 2016; Takács et al., 2017). When we injected embryos with CytoD or LatB, Patronin localized as small, dynamic puncta across the apical surface of cells, similar to myosin (Mason et al., 2013). Many of these Patronin puncta colocalized with myosin, suggesting a physical association between apical actomyosin and microtubules. While the importance of microtubules for apical constriction initiation could be tissue specific, it will be important to investigate if microtubules promote actomyosin connections to intercellular junctions in other developmental contexts.

We conclude that microtubules have a specific role for promoting actomyosin attachments to cell junctions for several reasons. The phenotype we observe is not consistent with a severe loss of E-cadherin–based adherens junctions, because (1) E-cadherin is still present apically at junctions and (2) actomyosin is able to engage with junctions and reattach after

separation, in contrast to mutant embryos with depleted junctions (Martin et al., 2010). While Dia was able to localize to junctions after microtubule disruption, we observed a depletion of Cno at junctions. Loss of Cno leads to a separation of actomyosin from junctions but prevents reattachment (Sawyer et al., 2009). Because actomyosin was able to reattach after microtubule disruption, loss of Cno localization may be a consequence of repeated separations of actomyosin from adherens junctions. Determining the precise mechanism by which microtubules promote F-actin meshwork repair and adherens junction attachment will be an important future area of study.

Materials and methods

Fly stocks and genetics

Fly stocks and crosses used in this study are listed in Table S1. Control (*rhodopsin-3*) and *patronin* knockdown flies were generated by crossing virgins of the shRNA lines to male flies carrying maternally loaded Gal4 drivers with appropriate markers. Crosses were maintained at 27°C. In the F2 generation, non-balancer females and males were used to set up cages that were incubated at 25°C. All other crosses and cages were maintained at 25°C.

Live and fixed imaging

For live imaging, embryos were dechorionated in 50% bleach, washed in water, and mounted onto a glass slide coated with glue (double-sided tape dissolved in heptane). Coverslips (No. 1.5) coated in glue were attached to the slide to use as spacers and a No. 1 coverslip was attached on top to create a chamber. Halocarbon 27 oil was used to fill the chamber. All imaging took place at room temperature (~23°C).

For fixed imaging, embryos were dechorionated in bleach, washed in water, and then fixed in 8% paraformaldehyde in 0.1 M phosphate buffer at pH 7.4 with 50% heptane for 30 min and manually devitellinized. For the best microtubule staining, embryos fixed in PFA were devitellinized by removing fixative, adding 50% methanol, and vortexing. These embryos were stored in 100% methanol at −20°C and rehydrated in 0.01% Tween 20 in PBS (PBS-T). In addition, some embryos (Fig. S3 B) were heat fixed in boiled Triton salt solution (0.03% Triton X-100 and 0.4% NaCl in water), cooled on ice, devitellinized in a 1:1 heptane/methanol solution, and stored and rehydrated as above.

Embryos were washed in PBS-T, blocked with 10% BSA in PBS-T, and incubated with antibodies diluted in PBS-T. To visualize F-actin, manually devitellinized embryos were incubated with Alexa Fluor 647–conjugated phalloidin (Invitrogen) diluted in 5% BSA in PBS-T overnight at 4°C. For PFA-fixed and manually devitellinized embryos, Asterless was recognized using antibody (a gift from J. Raff) diluted at 1:500, γ-Tubulin (GTU-88; Sigma-Aldrich) at 1:500, Dia (a gift from S. Wasserman) at 1:5000, and Cno (a gift from M. Peifer) at 1:500. For PFA-fixed embryos devitellinized by methanol addition and vortexing, α-Tubulin was recognized using antibody (Sigma-Aldrich) diluted at 1:500 and acetylated tubulin antibody (6-11B-1; Sigma-Aldrich) at 1:500. For heat-fixed embryos, Armadillo was recognized using antibody (Developmental Studies Hybridoma Bank) diluted 1:500 and Snail using antibody (a gift from M. Biggin) at 1:500. Embryos were incubated with primary antibodies at room temperature for 2 h. Secondary antibodies used were conjugated with Alexa Fluor 488, 568, or 647 (Invitrogen) diluted at 1:500 in 5% BSA in PBS-T incubated overnight at 4°C. Endogenous GFP signal was visualized for Patronin::GFP. After antibody incubation, embryos were mounted onto glass slides using AquaPolymount (Polysciences).

All images were taken on a Zeiss LSM 710 confocal microscope with a 40×/1.2 Apochromat water objective lens, an argon-ion, 561-nm diode, 594-nm HeNe, 633 HeNe laser, and Zen software. Pinhole settings ranged from 1 to 2.5 airy units. For two-color live imaging, band-pass filters were set at ~490–565 nm for GFP and ~590–690 nm for mCherry (mCH). For three-color imaging, band-pass filters were set at ~480–560 nm for GFP, ~580–635 nm for Alexa Fluor 568, and ~660–750 nm for Alexa Fluor 647.

Image processing and analysis

All images were processed using MATLAB (MathWorks) and FIJI (http://fiji.sc/wiki/index.php/Fiji). A Gaussian smoothing filter (kernel = 1 pixel) was applied. Apical projections are maximum-intensity Z-projections of multiple z sections (2–4 µm) and subapical sections are optical slices that are 1–2 µm below the apical sections.

Image segmentation for quantifications of cell area and myosin and Patronin intensities was performed using custom MATLAB software titled EDGE (Embryo Development Geometry Explorer; https://github.com/mgelbart/embryo-development-geometry-explorer; Gelbart et al., 2012). To calculate the junctional to medial ratio of Patronin::GFP intensity (Fig. 1 D), raw images were processed via background subtraction to remove cytoplasmic Patronin::GFP by subtracting the mean plus one half the standard deviation intensity value for the first time step from every pixel in all images. We made maximum-intensity projections via FIJI and imported the image stacks into EDGE. Cell boundaries were automatically detected and manually corrected, after which EDGE exported cell area and integrated intensity of Patronin::GFP for each cell. Medial Patronin::GFP intensity ($I_{M,Int}$) was defined as the integrated intensity value for the whole cell ($I_{W,Int}$), excluding the outermost two layers of pixels. Junctional Patronin::GFP intensity ($I_{J,Int}$) was calculated as the difference between $I_{W,Int}$ and $I_{M,Int}$. EDGE exported area values as total pixel numbers comprising the region of interest for both the whole cell (S_W) and the medial region (S_M). The area of the junctional region (S_J) was defined as the difference between S_W and S_M. Then, we proceeded to calculate the average pixel intensity of the junctional region (i_J) to that of the medial region (i_M) as follows:

$$r = \frac{i_J}{i_M} = \frac{I_{J,\,Int}}{I_{M,Int}} \times \frac{S_M}{S_J}.$$

We used average per-pixel intensity values instead of the integrated intensity values for that region to more accurately represent the local protein concentration. The same analysis was applied to calculate the junctional to medial ratio of E-cadherin::GFP intensity (Fig. 5 G).

To quantify changes in cell area and myosin intensity (Fig. 5, C and D), raw images were processed via background subtraction as described above. We made maximum-intensity projections via FIJI and imported the image stacks into EDGE. Cell boundaries were automatically detected and manually corrected, after which EDGE exported cell area and integrated intensity of Myosin::GFP for each cell. To calculate the cross-correlation between the rate of change in cell area constriction and per-pixel myosin intensity buildup rate (Fig. 5 D), we first smoothed the area and myosin integrated intensity curves of each cell by a moving average (three time steps wide) and then used these values to calculate the average per pixel intensity through time. Then, we found the rate of change in cell area constriction and per pixel myosin intensity buildup rate by finding the difference between a value at a given time step and the value two time steps prior and then dividing by the time difference and including only the time points between constriction initiation and mesoderm invagination. Finally, we used the MATLAB "xcorr" function to calculate the normalized cross-correlation between these two rates. We aggregated cross-correlation curves from multiple cells across three embryos from each condition (DMSO or Taxol injected) and obtained the average cross-correlation plot.

For the myosin and Patronin pulse analysis, we manually identified five myosin pulses in each of four embryos via FIJI and drew an elliptical region of interest around each pulse. We recorded the maximum pixel intensity in manually identified regions of interest for both. To plot the average relative behavior of the Myo::mCherry and Patronin::GFP signals (Fig. 3 C), we smoothed the intensity data for each pulse by a moving average (three time steps wide) and aligned them such that peak myosin intensity for all pulses would fall at a relative time offset of 0 s. Then, we calculated average Myo::mCherry and Patronin::GFP intensities for each relative time offset. We found the normalized cross-correlation between the rates of change in myosin intensity and Patronin intensity (Fig. 3 E) as indicated above.

Immunoblotting

Early gastrula stage embryos were collected and homogenized in SDS sample buffer, boiled for 5 min, and kept on ice. Samples were run on Mini-PROTEAN TGX Precast Gels (Bio-Rad). Primary antibodies used for immunoblotting included α-tubulin (1:500; Sigma-Aldrich) and Patronin (antibody serum; 1:50; a gift from Ron Vale). Primary antibodies were detected by horseradish peroxidase-labeled secondary antibodies. Signal was developed using SuperSignal West Femto Maximum Sensitivity Substrate (Thermo Fisher Scientific).

Drug injections

Dechorionated embryos were mounted onto glass slides and desiccated for 4 min using Drierite (Drierite). Embryos were covered with a 3:1 mixture of halocarbon 700/halocarbon 27 oils and then injected laterally during mid to late cellularization. For ROCK inhibition, Y-27632 was dissolved in water and injected at 50 mM concentration. 17 embryos were imaged, and quantifications in Fig. 4 B are from four representative embryos. As a control, water was injected. For RhoA inhibition, C3 exoenzyme protein (CT03; Cytoskeleton) was resuspended and dialyzed into PBS and injected at 1 mg/ml. 15 embryos were imaged and quantifications in Fig. 4 D are from four representative embryos. PBS was injected as a control. To depolymerize F-actin we resuspended CtyoD (Enzo Life Sciences) at either 5 mg/ml or 0.125 mg/ml in DMSO or LatB (Enzo Life Sciences) in DMSO (5 mg/ml). Colchicine and Taxol were both resuspended at 5 mg/ml in DMSO. Embryos were imaged 3–5 min after injection. For live injection of colchicine, embryos were mounted ventral side down onto a No.1 Coverslip. The embryo was pierced with the needle on the confocal microscope and injected after tissue folding had initiated during live imaging. To PFA fix embryos after injection, embryos were mounted onto a coverslip (No. 1.5) coated with a strip of glue. After injection, coverslips were placed into a Petri dish filled with heptane for ∼45 s to remove embryos from the glue. Embryos in heptane were transferred to a 10% paraformaldehyde solution in 0.1 M phosphate buffer at pH 7.4 with 50% heptane, fixed for 30 min, and manually devitellinized.

Online supplemental material

Fig. S1 shows the location of centrosomes, verification of *patronin*-RNAi, and the effect on microtubule organization after both genetic and pharmacological disruptions. Fig. S2 shows the effect of F-actin depolymerization on Patronin localization. Fig. S3 shows the phenotype of *patronin*-RNAi and the effect of Taxol on microtubule organization. Fig. S4 shows that myosin network separations can be repaired after microtubule disruption and does not affect medioapical ROCK polarity. In addition, the results of the live colchicine injection and the effect of microtubule disruption on E-cadherin polarity at later stages are shown. Video 1 shows the dynamic changes in localization of Patronin in the mesoderm and ectoderm. Video 2 shows the colocalization of myosin with dense patches of CLIP170. Video 3 shows the coalescence of Patronin, which spatiotemporally correlates with myosin pulses. Video 4 shows the phenotypes of microtubule drug injections on tissue invagination. Video 5 shows the dynamic myosin network separations after colchicine injection. Video 6 shows the effect on the F-actin meshwork after Taxol injection. Table S1 lists genotypes for all fly stocks and crosses used in this study.

Acknowledgments

We would like to thank members of the Martin laboratory for their helpful comments and suggestions on the project and the manuscript. We thank Frank Mason and Iain Cheeseman for their helpful comments on a draft of this manuscript. We would also like to thank Mark Biggin (Lawrence Berkeley National Laboratory, Berkeley, CA), Mark Peifer (University of North Carolina Chapel Hill, Chapel Hill, NC), Jordan Raff (University of Oxford, Oxford, UK), Ron Vale (University of California, San Francisco, San Francisco, CA), Steve Wasserman (University of California, San Diego, San Diego, CA), the Bloomington Stock Center, and TRiP at Harvard Medical School (National Institutes of Health/National Institute of General Medical Sciences grant R01-GM084947) for fly stocks and antibodies used in this study.

This work was supported by National Institute of General Medical Sciences grant R01GM105984 to A.C. Martin.

The authors declare no competing financial interests.

Author contributions: C.S. Ko and A.C. Martin conceptualized the project and designed experiments. C.S. Ko and A.C. Martin performed the experiments. C.S. Ko and V. Tserunyan analyzed the data. C.S. Ko and A.C. Martin wrote the manuscript. All authors reviewed and approved the final version of the manuscript.

Submitted: 2 February 2019
Revised: 30 April 2019
Accepted: 23 May 2019

References

Agarwal, P., and R. Zaidel-Bar. 2019. Principles of Actomyosin Regulation In Vivo. *Trends Cell Biol.* 29:150–163. https://doi.org/10.1016/j.tcb.2018.09.006

Amano, M., M. Ito, K. Kimura, Y. Fukata, K. Chihara, T. Nakano, Y. Matsuura, and K. Kaibuchi. 1996. Phosphorylation and activation of myosin by Rho-associated kinase (Rho-kinase). *J. Biol. Chem.* 271:20246–20249. https://doi.org/10.1074/jbc.271.34.20246

Applewhite, D.A., K.D. Grode, D. Keller, A.D. Zadeh, K.C. Slep, and S.L. Rogers. 2010. The spectraplakin Short stop is an actin-microtubule cross-linker that contributes to organization of the microtubule network. *Mol. Biol. Cell.* 21:1714–1724. https://doi.org/10.1091/mbc.e10-01-0011

Bacallao, R., C. Antony, C. Dotti, E. Karsenti, E.H. Stelzer, and K. Simons. 1989. The subcellular organization of Madin-Darby canine kidney cells during the formation of a polarized epithelium. *J. Cell Biol.* 109:2817–2832. https://doi.org/10.1083/jcb.109.6.2817

Barrett, K., M. Leptin, and J. Settleman. 1997. The Rho GTPase and a putative RhoGEF mediate a signaling pathway for the cell shape changes in Drosophila gastrulation. *Cell.* 91:905–915. https://doi.org/10.1016/S0092-8674(00)80482-1

Blanchard, G.B., S. Murugesu, R.J. Adams, A. Martinez-Arias, and N. Gorfinkiel. 2010. Cytoskeletal dynamics and supracellular organisation of cell shape fluctuations during dorsal closure. *Development.* 137:2743–2752. https://doi.org/10.1242/dev.045872

Booth, A.J.R., G.B. Blanchard, R.J. Adams, and K. Röper. 2014. A dynamic microtubule cytoskeleton directs medial actomyosin function during tube formation. *Dev. Cell.* 29:562–576. https://doi.org/10.1016/j.devcel.2014.03.023

Chanet, S., R. Sharan, Z. Khan, and A.C. Martin. 2017. Myosin 2-Induced Mitotic Rounding Enables Columnar Epithelial Cells to Interpret Cortical Spindle Positioning Cues. *Curr. Biol.* 27:3350–3358.e3. https://doi.org/10.1016/j.cub.2017.09.039

Choi, W., B.R. Acharya, G. Peyret, M.-A. Fardin, R.-M. Mège, B. Ladoux, A.S. Yap, A.S. Fanning, and M. Peifer. 2016. Remodeling the zonula adherens in response to tension and the role of afadin in this response. *J. Cell Biol.* 213:243–260. https://doi.org/10.1083/jcb.201506115

Chung, S., S. Kim, and D.J. Andrew. 2017. Uncoupling apical constriction from tissue invagination. *eLife.* 6:e22235. https://doi.org/10.7554/eLife.22235

Coravos, J.S., and A.C. Martin. 2016. Apical Sarcomere-like Actomyosin Contracts Nonmuscle Drosophila Epithelial Cells. *Dev. Cell.* 39:346–358. https://doi.org/10.1016/j.devcel.2016.09.023

Costa, M., E.T. Wilson, and E. Wieschaus. 1994. A putative cell signal encoded by the *folded gastrulation* gene coordinates cell shape changes during Drosophila gastrulation. *Cell.* 76:1075–1089. https://doi.org/10.1016/0092-8674(94)90384-0

Crawford, J.M., N. Harden, T. Leung, L. Lim, and D.P. Kiehart. 1998. Cellularization in *Drosophila melanogaster* is disrupted by the inhibition of rho activity and the activation of Cdc42 function. *Dev. Biol.* 204:151–164. https://doi.org/10.1006/dbio.1998.9061

David, D.J.V., A. Tishkina, and T.J.C. Harris. 2010. The PAR complex regulates pulsed actomyosin contractions during amnioserosa apical constriction in Drosophila. *Development.* 137:1645–1655. https://doi.org/10.1242/dev.044107

Davies, S.P., H. Reddy, M. Caivano, and P. Cohen. 2000. Specificity and mechanism of action of some commonly used protein kinase inhibitors. *Biochem. J.* 351:95–105. https://doi.org/10.1042/bj3510095

Dawes-Hoang, R.E., K.M. Parmar, A.E. Christiansen, C.B. Phelps, A.H. Brand, and E.F. Wieschaus. 2005. *folded gastrulation*, cell shape change and the control of myosin localization. *Development.* 132:4165–4178. https://doi.org/10.1242/dev.01938

Desai, R., R. Sarpal, N. Ishiyama, M. Pellikka, M. Ikura, and U. Tepass. 2013. Monomeric α-catenin links cadherin to the actin cytoskeleton. *Nat. Cell Biol.* 15:261–273. https://doi.org/10.1038/ncb2685

Dictenberg, J.B., W. Zimmerman, C.A. Sparks, A. Young, C. Vidair, Y. Zheng, W. Carrington, F.S. Fay, and S.J. Doxsey. 1998. Pericentrin and γ-tubulin form a protein complex and are organized into a novel lattice at the centrosome. *J. Cell Biol.* 141:163–174. https://doi.org/10.1083/jcb.141.1.163

Dzhindzhev, N.S., Q.D. Yu, K. Weiskopf, G. Tzolovsky, I. Cunha-Ferreira, M. Riparbelli, A. Rodrigues-Martins, M. Bettencourt-Dias, G. Callaini, and D.M. Glover. 2010. Asterless is a scaffold for the onset of centriole assembly. *Nature.* 467:714–718. https://doi.org/10.1038/nature09445

Evangelista, M., K. Blundell, M.S. Longtine, C.J. Chow, N. Adames, J.R. Pringle, M. Peter, and C. Boone. 1997. Bnilp, a yeast formin linking cdc42p and the actin cytoskeleton during polarized morphogenesis. *Science.* 276:118–122. https://doi.org/10.1126/science.276.5309.118

Fernandez-Gonzalez, R., S.M. Simoes, J.-C. Röper, S. Eaton, and J.A. Zallen. 2009. Myosin II dynamics are regulated by tension in intercalating cells. *Dev. Cell.* 17:736–743. https://doi.org/10.1016/j.devcel.2009.09.003

Fox, D.T., and M. Peifer. 2007. Abelson kinase (Abl) and RhoGEF2 regulate actin organization during cell constriction in Drosophila. *Development.* 134:567–578. https://doi.org/10.1242/dev.02748

Gelbart, M.A., B. He, A.C. Martin, S.Y. Thiberge, E.F. Wieschaus, and M. Kaschube. 2012. Volume conservation principle involved in cell lengthening and nucleus movement during tissue morphogenesis. *Proc. Natl. Acad. Sci. USA.* 109:19298–19303. https://doi.org/10.1073/pnas.1205258109

Girdler, G.C., D.A. Applewhite, W.M.G. Perry, S.L. Rogers, and K. Röper. 2016. The Gas2 family protein Pigs is a microtubule +TIP that affects cytoskeleton organisation. *J. Cell Sci.* 129:121–134. https://doi.org/10.1242/jcs.176230

Goodwin, S.S., and R.D. Vale. 2010. Patronin regulates the microtubule network by protecting microtubule minus ends. *Cell.* 143:263–274. https://doi.org/10.1016/j.cell.2010.09.022

Grosshans, J., C. Wenzl, H.-M. Herz, S. Bartoszewski, F. Schnorrer, N. Vogt, H. Schwarz, and H.A. Müller. 2005. RhoGEF2 and the formin Dia control the formation of the furrow canal by directed actin assembly during Drosophila cellularisation. *Development.* 132:1009–1020. https://doi.org/10.1242/dev.01669

Häcker, U., and N. Perrimon. 1998. DRhoGEF2 encodes a member of the Dbl family of oncogenes and controls cell shape changes during gastrulation in Drosophila. *Genes Dev.* 12:274–284. https://doi.org/10.1101/gad.12.2.274

Harris, T.J.C., and M. Peifer. 2005. The positioning and segregation of apical cues during epithelial polarity establishment in *Drosophila*. *J. Cell Biol.* 170:813–823. https://doi.org/10.1083/jcb.200505127

Harris, T.J.C., and M. Peifer. 2007. aPKC controls microtubule organization to balance adherens junction symmetry and planar polarity during development. *Dev. Cell.* 12:727–738. https://doi.org/10.1016/j.devcel.2007.02.011

Heisenberg, C.-P., and Y. Bellaïche. 2013. Forces in tissue morphogenesis and patterning. *Cell.* 153:948–962. https://doi.org/10.1016/j.cell.2013.05.008

Hendershott, M.C., and R.D. Vale. 2014. Regulation of microtubule minus-end dynamics by CAMSAPs and Patronin. *Proc. Natl. Acad. Sci. USA.* 111:5860–5865. https://doi.org/10.1073/pnas.1404133111

Henty-Ridilla, J.L., A. Rankova, J.A. Eskin, K. Kenny, and B.L. Goode. 2016. Accelerated actin filament polymerization from microtubule plus ends. *Science.* 352:1004–1009. https://doi.org/10.1126/science.aaf1709

Izquierdo, E., T. Quinkler, and S. De Renzis. 2018. Guided morphogenesis through optogenetic activation of Rho signalling during early Drosophila embryogenesis. *Nat. Commun.* 9:2366. https://doi.org/10.1038/s41467-018-04754-z

Jaffe, A.B., and A. Hall. 2005. Rho GTPases: Biochemistry and biology. *Annu. Rev. Cell Dev. Biol.* 21:247–269. https://doi.org/10.1146/annurev.cellbio.21.020604.150721

Jiang, K., S. Hua, R. Mohan, I. Grigoriev, K.W. Yau, Q. Liu, E.A. Katrukha, A.F. Altelaar, A.J.R. Heck, C.C. Hoogenraad, and A. Akhmanova. 2014. Microtubule minus-end stabilization by polymerization-driven CAMSAP deposition. *Dev. Cell.* 28:295–309. https://doi.org/10.1016/j.devcel.2014.01.001

Jodoin, J.N., J.S. Coravos, S. Chanet, C.G. Vasquez, M. Tworoger, E.R. Kingston, L.A. Perkins, N. Perrimon, and A.C. Martin. 2015. Stable Force Balance between Epithelial Cells Arises from F-Actin Turnover. *Dev. Cell.* 35:685–697. https://doi.org/10.1016/j.devcel.2015.11.018

Kasza, K.E., and J.A. Zallen. 2011. Dynamics and regulation of contractile actin-myosin networks in morphogenesis. *Curr. Opin. Cell Biol.* 23: 30–38. https://doi.org/10.1016/j.ceb.2010.10.014

Khanal, I., A. Elbediwy, M.C. Diaz de la Loza, G.C. Fletcher, and B.J. Thompson. 2016. Shot and Patronin polarise microtubules to direct membrane traffic and biogenesis of microvilli in epithelia. *J. Cell Sci.* 129: 2651–2659. https://doi.org/10.1242/jcs.189076

King, M.D.A., G.W. Phillips, P.A. Bignone, N.V.L. Hayes, J.C. Pinder, and A.J. Baines. 2014. A conserved sequence in calmodulin regulated spectrin-associated protein 1 links its interaction with spectrin and calmodulin to neurite outgrowth. *J. Neurochem.* 128:391–402. https://doi.org/10.1111/jnc.12462

Kölsch, V., T. Seher, G.J. Fernandez-Ballester, L. Serrano, and M. Leptin. 2007. Control of *Drosophila* gastrulation by apical localization of adherens junctions and RhoGEF2. *Science.* 315:384–386. https://doi.org/10.1126/science.1134833

Lecuit, T., and A.S. Yap. 2015. E-cadherin junctions as active mechanical integrators in tissue dynamics. *Nat. Cell Biol.* 17:533–539. https://doi.org/10.1038/ncb3136

Lecuit, T., P.-F. Lenne, and E. Munro. 2011. Force generation, transmission, and integration during cell and tissue morphogenesis. *Annu. Rev. Cell Dev. Biol.* 27:157–184. https://doi.org/10.1146/annurev-cellbio-100109-104027

Le Droguen, P.-M., S. Claret, A. Guichet, and V. Brodu. 2015. Microtubule-dependent apical restriction of recycling endosomes sustains adherens junctions during morphogenesis of the Drosophila tracheal system. *Development.* 142:363–374. https://doi.org/10.1242/dev.113472

Lee, J.-Y., and R.M. Harland. 2007. Actomyosin contractility and microtubules drive apical constriction in Xenopus bottle cells. *Dev. Biol.* 311: 40–52. https://doi.org/10.1016/j.ydbio.2007.08.010

Lee, C., H.M. Scherr, and J.B. Wallingford. 2007. Shroom family proteins regulate gamma-tubulin distribution and microtubule architecture during epithelial cell shape change. *Development.* 134:1431–1441. https://doi.org/10.1242/dev.02828

Leptin, M., and B. Grunewald. 1990. Cell shape changes during gastrulation in *Drosophila*. *Development.* 110:73–84.

López, M.P., F. Huber, I. Grigoriev, M.O. Steinmetz, A. Akhmanova, G.H. Koenderink, and M. Dogterom. 2014. Actin-microtubule coordination at growing microtubule ends. *Nat. Commun.* 5:4778.

Marston, D.J., C.D. Higgins, K.A. Peters, T.D. Cupp, D.J. Dickinson, A.M. Pani, R.P. Moore, A.H. Cox, D.P. Kiehart, and B. Goldstein. 2016. MRCK-1 Drives Apical Constriction in *C. elegans* by Linking Developmental Patterning to Force Generation. *Curr. Biol.* 26:2079–2089. https://doi.org/10.1016/j.cub.2016.06.010

Martin, A.C., and B. Goldstein. 2014. Apical constriction: Themes and variations on a cellular mechanism driving morphogenesis. *Development.* 141: 1987–1998. https://doi.org/10.1242/dev.102228

Martin, A.C., M. Kaschube, and E.F. Wieschaus. 2009. Pulsed contractions of an actin-myosin network drive apical constriction. *Nature.* 457: 495–499. https://doi.org/10.1038/nature07522

Martin, A.C., M. Gelbart, R. Fernandez-Gonzalez, M. Kaschube, and E.F. Wieschaus. 2010. Integration of contractile forces during tissue invagination. *J. Cell Biol.* 188:735–749. https://doi.org/10.1083/jcb.200910099

Mason, F.M., M. Tworoger, and A.C. Martin. 2013. Apical domain polarization localizes actin-myosin activity to drive ratchet-like apical constriction. *Nat. Cell Biol.* 15:926–936. https://doi.org/10.1038/ncb2796

Mason, F.M., S. Xie, C.G. Vasquez, M. Tworoger, and A.C. Martin. 2016. RhoA GTPase inhibition organizes contraction during epithelial morphogenesis. *J. Cell Biol.* 214:603–617. https://doi.org/10.1083/jcb.201603077

Meng, W., Y. Mushika, T. Ichii, and M. Takeichi. 2008. Anchorage of microtubule minus ends to adherens junctions regulates epithelial cell-cell contacts. *Cell.* 135:948–959. https://doi.org/10.1016/j.cell.2008.09.040

Michael, M., J.C.M. Meiring, B.R. Acharya, D.R. Matthews, S. Verma, S.P. Han, M.M. Hill, R.G. Parton, G.A. Gomez, and A.S. Yap. 2016. Coronin 1B Reorganizes the Architecture of F-Actin Networks for Contractility at Steady-State and Apoptotic Adherens Junctions. *Dev. Cell.* 37:58–71. https://doi.org/10.1016/j.devcel.2016.03.008

Mizuno, T., M. Amano, K. Kaibuchi, and Y. Nishida. 1999. Identification and characterization of *Drosophila* homolog of Rho-kinase. *Gene.* 238: 437–444. https://doi.org/10.1016/S0378-1119(99)00351-0

Mogensen, M.M., A. Malik, M. Piel, V. Bouckson-Castaing, and M. Bornens. 2000. Microtubule minus-end anchorage at centrosomal and non-centrosomal sites: The role of ninein. *J. Cell Sci.* 113:3013–3023.

Moss, D.K., G. Bellett, J.M. Carter, M. Liovic, J. Keynton, A.R. Prescott, E.B. Lane, and M.M. Mogensen. 2007. Ninein is released from the centrosome and moves bi-directionally along microtubules. *J. Cell Sci.* 120: 3064–3074. https://doi.org/10.1242/jcs.010322

Munjal, A., J.-M. Philippe, E. Munro, and T. Lecuit. 2015. A self-organized biomechanical network drives shape changes during tissue morphogenesis. *Nature.* 524:351–355. https://doi.org/10.1038/nature14603

Munro, E., J. Nance, and J.R. Priess. 2004. Cortical flows powered by asymmetrical contraction transport PAR proteins to establish and maintain anterior-posterior polarity in the early C. elegans embryo. *Dev. Cell.* 7: 413–424. https://doi.org/10.1016/j.devcel.2004.08.001

Murrell, M., P.W. Oakes, M. Lenz, and M.L. Gardel. 2015. Forcing cells into shape: The mechanics of actomyosin contractility. *Nat. Rev. Mol. Cell Biol.* 16:486–498. https://doi.org/10.1038/nrm4012

Nagae, S., W. Meng, and M. Takeichi. 2013. Non-centrosomal microtubules regulate F-actin organization through the suppression of GEF-H1 activity. *Genes Cells.* 18:387–396. https://doi.org/10.1111/gtc.12044

Nashchekin, D., A.R. Fernandes, and D. St Johnston. 2016. Patronin/Shot Cortical Foci Assemble the Noncentrosomal Microtubule Array that Specifies the Drosophila Anterior-Posterior Axis. *Dev. Cell.* 38:61–72. https://doi.org/10.1016/j.devcel.2016.06.010

Noordstra, I., Q. Liu, W. Nijenhuis, S. Hua, K. Jiang, M. Baars, S. Remmelzwaal, M. Martin, L.C. Kapitein, and A. Akhmanova. 2016. Control of apico-basal epithelial polarity by the microtubule minus-end-binding protein CAMSAP3 and spectraplakin ACF7. *J. Cell Sci.* 129:4278–4288. https://doi.org/10.1242/jcs.194878

Otomo, T., C. Otomo, D.R. Tomchick, M. Machius, and M.K. Rosen. 2005. Structural basis of Rho GTPase-mediated activation of the formin mDia1. *Mol. Cell.* 18:273–281. https://doi.org/10.1016/j.molcel.2005.04.002

Perez, F., G.S. Diamantopoulos, R. Stalder, and T.E. Kreis. 1999. CLIP-170 highlights growing microtubule ends in vivo. *Cell.* 96:517–527. https://doi.org/10.1016/S0092-8674(00)80656-X

Rauzi, M., P.-F. Lenne, and T. Lecuit. 2010. Planar polarized actomyosin contractile flows control epithelial junction remodelling. *Nature.* 468: 1110–1114. https://doi.org/10.1038/nature09566

Rogers, S.L., U. Wiedemann, U. Häcker, C. Turck, and R.D. Vale. 2004. Drosophila RhoGEF2 associates with microtubule plus ends in an EB1-dependent manner. *Curr. Biol.* 14:1827–1833. https://doi.org/10.1016/j.cub.2004.09.078

Roh-Johnson, M., G. Shemer, C.D. Higgins, J.H. McClellan, A.D. Werts, U.S. Tulu, L. Gao, E. Betzig, D.P. Kiehart, and B. Goldstein. 2012. Triggering a cell shape change by exploiting preexisting actomyosin contractions. *Science.* 335:1232–1235. https://doi.org/10.1126/science.1217869

Royou, A., W. Sullivan, and R. Karess. 2002. Cortical recruitment of non-muscle myosin II in early syncytial Drosophila embryos. *J. Cell Biol.* 158: 127–137. https://doi.org/10.1083/jcb.200203148

Salmon, W.C., M.C. Adams, and C.M. Waterman-Storer. 2002. Dual-wavelength fluorescent speckle microscopy reveals coupling of microtubule and actin movements in migrating cells. *J. Cell Biol.* 158:31–37. https://doi.org/10.1083/jcb.200203022

Sánchez-Corrales, Y.E., G.B. Blanchard, and K. Röper. 2018. Radially patterned cell behaviours during tube budding from an epithelium. *eLife.* 7: e35717. https://doi.org/10.7554/eLife.35717

Sawyer, J.K., N.J. Harris, K.C. Slep, U. Gaul, and M. Peifer. 2009. The Drosophila afadin homologue Canoe regulates linkage of the actin cytoskeleton to adherens junctions during apical constriction. *J. Cell Biol.* 186:57–73. https://doi.org/10.1083/jcb.200904001

Sawyer, J.M., J.R. Harrell, G. Shemer, J. Sullivan-Brown, M. Roh-Johnson, and B. Goldstein. 2010. Apical constriction: A cell shape change that can drive morphogenesis. *Dev. Biol.* 341:5–19. https://doi.org/10.1016/j.ydbio.2009.09.009

Sawyer, J.K., W. Choi, K.-C. Jung, L. He, N.J. Harris, and M. Peifer. 2011. A contractile actomyosin network linked to adherens junctions by Canoe/afadin helps drive convergent extension. *Mol. Biol. Cell.* 22:2491–2508. https://doi.org/10.1091/mbc.e11-05-0411

Singh, A., T. Saha, I. Begemann, A. Ricker, H. Nüsse, O. Thorn-Seshold, J. Klingauf, M. Galic, and M. Matis. 2018. Polarized microtubule dynamics directs cell mechanics and coordinates forces during epithelial morphogenesis. *Nat. Cell Biol.* 20:1126–1133. https://doi.org/10.1038/s41556-018-0193-1

Stehbens, S.J., A.D. Paterson, M.S. Crampton, A.M. Shewan, C. Ferguson, A. Akhmanova, R.G. Parton, and A.S. Yap. 2006. Dynamic microtubules regulate the local concentration of E-cadherin at cell-cell contacts. *J. Cell Sci.* 119:1801–1811. https://doi.org/10.1242/jcs.02903

Sweeton, D., S. Parks, M. Costa, and E. Wieschaus. 1991. Gastrulation in *Drosophila:* The formation of the ventral furrow and posterior midgut invaginations. *Development.* 112:775–789.

Takács, Z., F. Jankovics, P. Vilmos, P. Lénárt, K. Röper, and M. Erdélyi. 2017. The spectraplakin Short stop is an essential microtubule regulator involved in epithelial closure in *Drosophila*. *J. Cell Sci.* 130:712–724. https://doi.org/10.1242/jcs.193003

Takeda, M., M.M. Sami, and Y.C. Wang. 2018. A homeostatic apical microtubule network shortens cells for epithelial folding via a basal polarity shift. *Nat. Cell Biol.* 20:36–45. https://doi.org/10.1038/s41556-017-0001-3

Tanaka, N., W. Meng, S. Nagae, and M. Takeichi. 2012. Nezha/CAMSAP3 and CAMSAP2 cooperate in epithelial-specific organization of noncentrosomal microtubules. *Proc. Natl. Acad. Sci. USA.* 109:20029–20034. https://doi.org/10.1073/pnas.1218017109

Toya, M., S. Kobayashi, M. Kawasaki, G. Shioi, M. Kaneko, T. Ishiuchi, K. Misaki, W. Meng, and M. Takeichi. 2016. CAMSAP3 orients the apical-to-basal polarity of microtubule arrays in epithelial cells. *Proc. Natl. Acad. Sci. USA.* 113:332–337. https://doi.org/10.1073/pnas.1520638113

Varmark, H., S. Llamazares, E. Rebollo, B. Lange, J. Reina, H. Schwarz, and C. Gonzalez. 2007. Asterless is a centriolar protein required for centrosome function and embryo development in *Drosophila*. *Curr. Biol.* 17:1735–1745. https://doi.org/10.1016/j.cub.2007.09.031

Vasquez, C.G., M. Tworoger, and A.C. Martin. 2014. Dynamic myosin phosphorylation regulates contractile pulses and tissue integrity during epithelial morphogenesis. *J. Cell Biol.* 206:435–450. https://doi.org/10.1083/jcb.201402004

Watanabe, N., P. Madaule, T. Reid, T. Ishizaki, G. Watanabe, A. Kakizuka, Y. Saito, K. Nakao, B.M. Jockusch, and S. Narumiya. 1997. p140mDia, a mammalian homolog of Drosophila diaphanous, is a target protein for Rho small GTPase and is a ligand for profilin. *EMBO J.* 16:3044–3056. https://doi.org/10.1093/emboj/16.11.3044

Weng, M., and E. Wieschaus. 2016. Myosin-dependent remodeling of adherens junctions protects junctions from Snail-dependent disassembly. *J. Cell Biol.* 212:219–229. https://doi.org/10.1083/jcb.201508056

Westermann, S., and K. Weber. 2003. Post-translational modifications regulate microtubule function. *Nat. Rev. Mol. Cell Biol.* 4:938–947. https://doi.org/10.1038/nrm1260